https://doi.org/10.5194/egusphere-2026-4611
Preprint. Discussion started: 9 November 2026
© Author(s) 2026. CC BY 4.0 License.

Evaluation of a simplified double-moment aerosol scheme (SOL/INSOL) using satellite, airborne and ground based observations over the UK

Angela Mynard[1], Anthony C. Jones[1], Joseph Carton-Kelly[1], Paul Field[1,2], Steven J Abel[1,2], and Florent Fabien Malavelle[1]

[1]Met Office, Exeter, UK
[2]School of Earth, Environment and Sustainability, University of Leeds, UK

Correspondence: Angela Mynard (angela.mynard@metoffice.gov.uk)

Abstract. Uncertainty in aerosol processes, particularly aerosol–cloud interactions (ACI), remains high, limiting the predictive skill of clouds and rainfall across timescales. Aerosols also contribute to visibility degradation, highlighting the need for accurate forecasts to support safety and reduce transport-related economic impacts. Consequently, the development of consistent, scalable, and computationally affordable aerosol representations that are applicable across both numerical weather prediction and climate timescales is increasingly important.

To this end, we introduce and evaluate a new double-moment prognostic aerosol scheme, named SOL/INSOL ("SOLuble and INSOLuble"), implemented within the Met Office's UKV local area model. SOL/INSOL is a simplified configuration of the United Kingdom Aerosol and Chemistry used for climate projections. A global driving model provides lateral boundary conditions to the UKV, where aerosol precursor fields are initialized using the Copernicus Atmosphere Monitoring Service (CAMS) reanalysis dataset. Emissions ancillaries are monthly means used in the Met Office operational air quality model. This development enables coupling of number concentration with the UKV cloud microphysics scheme, CASIM, which will strengthen the model's treatment of ACI.

This study presents an in-depth evaluation of simulated SOL/INSOL $PM_{2.5}$ using surface and airborne $PM_{2.5}$ observations, alongside a comparison of modeled aerosol optical depth with satellite retrievals for a selected case date. We then run a suite of case studies amounting to 31 dates over the UK which are compared to both UK-wide ground sites, and regional airborne observations over Manchester, London and Birmingham. We also perform sensitivity simulations, and evaluate the short-term forecasting skill of the model. Model skill is quantified in terms of normalised mean bias (NMB).

We show that SOL/INSOL predicts $PM_{2.5}$ with fidelity, reproducing surface $PM_{2.5}$ mass concentrations to within 13% of that observed. We show that using CAMS reanalysis for initial conditions perform well, demonstrating how variations in the relative contributions of these gridded precursor aerosol components translate into systematic changes in modal particle size distributions and associated $PM_{2.5}$ concentrations. Our simulations investigating sensitivity to lead time show that SOL/INSOL has good predictive skill up to T+37 hours. We show that the simulated number concentrations agree well with observations, providing confidence in their use within the UKV cloud microphysics scheme. We find that SOL/INSOL is currently limited in its ability to accurately reproduce discrete, localised enhanced aerosol events and discuss future requirements to address this

https://doi.org/10.5194/egusphere-2026-4611
Preprint. Discussion started: 9 November 2026
© Author(s) 2026. CC BY 4.0 License.



shortfall. We conclude that the simple aerosol scheme shows excellent promise for further testing in operational forecasting at the UK Met Office.

1 Introduction

The impacts of atmospheric aerosol on Earth's climate are manifold and far reaching across varying temporal and spatial scales, from regional impacts that affect society and human health such as air quality (Jayakumar et al., 2025) to global climate forcing and impacts on cloud properties (Bellouin et al., 2019). Aerosol processes are also implicated in weather phenomena such as visibility degradation, where accurate forecasting is essential for ensuring safety and minimising economic impacts, particularly in the transport industry (Clark et al., 2008). Uncertainty in aerosol processes is high, and aerosol-cloud interactions (ACI) and associated radiative forcing remains one of the largest uncertainties in climate prediction (Mikkelsen et al., 2025). High resolution Numerical Weather Prediction (NWP) models coupled with aerosol models are increasingly used to challenge and develop parametrisations used in coarse resolution global climate models (GCMs) (Gordon et al. (2023), Ghosh et al. (2025)). Therefore, a consistent and scalable representation of aerosol that works on both NWP and climate timescales is increasingly important to meteorological centres with weather and climate interests such as the UK Met Office.

Nested-domain Local Area Models (LAMs) run at NWP timescales (days to weeks) naturally have higher spatio-temporal fidelity and can resolve more atmospheric processes, which makes them a useful tool for evaluating aerosol microphysics and chemistry (Gordon et al., 2023). LAMs are increasingly run with chemistry and aerosol representation (e.g., Gao and Zhou (2024), Wang et al. (2025)). A common usage of these models is to utilise spatio-temporally-constrained observations (e.g. field campaigns, surface sites) and specific weather case-studies to develop and test parametrisations such as the impact of absorbing aerosol impacts on fog blankets (Anurose et al., 2024), volatile organic aerosol formation based on a Los Angeles case study (Zhu et al., 2024), aerosol-mediated fog formation over Paris (Ghosh et al., 2025) or to create training data for ML air quality emulators (Yang et al., 2025). Alternatively, LAMS coupled to aerosol models are used operationally for Air Quality forecasts such as the 300m resolution DM-chem over Delhi (Jayakumar et al., 2025).

Running LAMs that explicitly represent aerosol processes (chemistry, cloud, and radiation interactions) is computationally demanding and often simplified aerosol schemes are sought that limit computational cost (Warren et al., 2020). This problem is not limited to NWP simulations, and global kilometre-scale models are also turning to simplified aerosol such as HAM-lite developed for ICON (Weiss et al., 2024). Even simplistic bulk-mass aerosol models require the advection of numerous tracers and often make sacrifices, e.g.: to spatiotemporal resolution (Neal et al., 2017). Nevertheless, the advantages of running double-moment aerosol schemes (which employ predictions of the 0th and 3rd moments) capable of accurately modelling aerosol size properties, to drive hydrology is clear. ACI processes of cloud droplet activation, autoconversion, and fog droplet formation are highly sensitive to the size and number concentration of ambient aerosols and require sectional or modal aerosol models (Dedrick et al., 2024; Yan et al., 2021). Therefore, there appears inherent value in accurately representing the aerosol size distribution in the simulation of salient hydrological features such as rain and cloud cover in NWP forecasts (e.g.: Cao et al. (2021)).

https://doi.org/10.5194/egusphere-2026-4611
Preprint. Discussion started: 9 November 2026
© Author(s) 2026. CC BY 4.0 License.

For Met Office weather forecasts, the MURK aerosol scheme (Clark et al., 2008) has been used operationally since 2008 to diagnose visibility (fog) and cloud drop concentration, before the recent upgrade to the Cloud AeroSol Interacting Microphysics (CASIM) cloud microphysics scheme in the Regional Atmosphere and Land model 3 (RAL3, Field et al. (2023), Bush et al. (2025)). MURK is a single bulk-mass tracer with fixed size distribution and therefore unable to represent the complex aerosol processing in the atmosphere. This persistent reliance on MURK means that, given present operational configurations, dynamic and thermodynamic representation improves with increases in resolution, but the aerosol and composition detail stagnates. More computationally efficient aerosol schemes that capture an appropriate level of complexity are needed to accurately drive hydrology, particularly in light of the incorporation of double moment cloud-microphysics and improved simulation of cloud and precipitation microphysics, as well as in the move to higher resolution models.

To this end, we introduce the double-moment SOL/INSOL prognostic aerosol scheme, a configuration of the UK Chemistry and Aerosol composition-climate submodel (UKCA, Morgenstern et al. (2009)) that simplifies aerosol representation to a single species (sulphate) across 4 soluble modes and a single species (desert dust) across 2 insoluble modes. SOL/INSOL is intended for NWP simulations and aims to be the operational aerosol model for visibility and cloud droplet activation in the Met Office UKV model. The aims of this study are foundational: to introduce SOL/INSOL and evaluate predicted particulate matter with a diameter ≤ 2.5 μm ($PM_{2.5}$) size distributions, mass burdens and spatial trends during clear sky cases over the southern United Kingdom, against ground, airborne and satellite observations. Of particular importance is demonstrating the impact of the simplified aerosol scheme, ensuring fundamental aerosol are represented with fidelity. This evaluation also presents an opportunity to utilise the unique UKRI Special Priorities Fund (SPF) Met Office Atmospheric Survey Aircraft (MOASA) Clean Air Project (hereonin referred to as "MCAP") dataset which provides unparalleled regional observations of the three-dimensional distribution of air pollutants (Mynard et al., 2023). A single MCAP case has been identified for comprehensive evaluation, with a further 30 MCAP cases included to enhance robustness of the statistical assessment.

This report proceeds as follows: the SOL/INSOL aerosol scheme is described in section 2. An overview of observational methods and data is given in section 3 and selected case studies are summarised in section 4. Evaluation against observations, where model skill is quantified in terms of normalised mean bias (NMB) are presented in section 5. This section includes nationwide (5.1) and regional (5.2) analysis and sensitivity simulations (5.3). We investigate the sensitivity to forecast lead time in section 5.4. Finally, we conclude and discuss future developments in section 6.

2 Model description

SOL/INSOL is integrated within the Met Office Unified Model (UM). The UM employs the Joint UK Land Environment Simulator (JULES, Bush et al. (2025)) land surface model, in a multi-scale framework, using a global driving model (GLM) to provide lateral boundary conditions to the United Kingdom Variable Resolution (UKV) LAM. The UKV is the UK Met Office's current operational deterministic weather forecast system, which is well-validated and demonstrates useful fidelity (e.g.: Tang et al. (2013), Bohnenstengel and Hendry (2016)). The UKV uses the Regional Atmosphere and Land 3.3 (RAL3.3) science configuration. Developments within the RAL3 configuration include a bimodal cloud scheme, updates to the boundary layer

https://doi.org/10.5194/egusphere-2026-4611
Preprint. Discussion started: 9 November 2026
© Author(s) 2026. CC BY 4.0 License.

and land surface options (see Bush et al. (2025) for details) and, of particualar relevance to this work, the addition of CASIM, a multi-moment bulk microphysics scheme which can represent cloud microphysics processes and aerosol–cloud interactions across spatial and temporal scales (Field et al., 2023).

In the standard RAL3 configuration, CASIM is implemented as a two-moment scheme wherein mass mixing ratios and the shape of the size distribution vary between grid-boxes while the in-cloud droplet number concentration is fixed. CASIM can alternatively be run with prognostic droplet number concentration derived from aerosol fields, an option that depends on having sufficiently skilful aerosol concentration predictions (Bush et al., 2025). This dependency is a key motivation behind the development of SOL/INSOL which will link aerosol to droplet number concentration. For this study, the UKV is run with 1-way coupling between CASIM and the UKCA submodel. Aerosol size distribution and composition is represented using the SOL/INSOL aerosol scheme. The nucleation and subcloud scavenging processes are treated within SOL/INSOL, while cloud droplet activation is parameterised in CASIM using Abdul-Razzak and Ghan (2000). A postliminary review is currently underway examining the 2-way coupling of SOL/INSOL with CASIM (where aerosol fields are provided by SOL/INSOL, passed to CASIM and returned back to aerosol following cloud processing) and its implications for ACI and hydrology.

The UKV simulations presented here employ a 1.5km variable grid LAM that stretches to 4.5 km at the edges of the domain (Field et al., 2023), centered over the UK and Ireland (622 x 810 latitude, longitude points in the inner area). The UKV model uses a hybrid height vertical coordinate system with 70 levels up to the model top at 40 km, where to increase resolution near the surface, the lowest 1 km of the atmosphere contains 16 levels. For this study, output is 6-hourly. The UKV timestep is 60 seconds, with chemistry called every 15th timestep. Microphysics is called 6 times per chemistry timestep (every 2.5 minutes) allowing high resolution bi-directional coupling between chemistry and aerosols to represent the competition (Mann et al., 2010) of nucleation, coagulation, and condensational growth processes (section 2.3).

2.1 SOL/INSOL Aerosol

Size distribution and composition of aerosol particles is represented in the UKCA using the SOL/INSOL aerosol scheme. SOL/INSOL adopts a modal aerosol dynamics approach, where the shape of the particle size distribution is parametrized as a series of log-normal modes which cover defined regions of the particle size range (Mann et al., 2010). As a double-moment scheme, modal number and component mass concentrations vary between grid-boxes and the modal width (see figure **??**) is fixed. SOL/INSOL has four soluble modes in the nucleation, Aitken, accumulation and coarse ranges. Rather than employing more complex dust schemes such as the 3 mode dust scheme intended for use in UKESM2 (Earth System Model 2, developed with GA8 and UKCA and prepared for CMIP7, in development) or the extensively utilized CLASSIC dust scheme (Woodward, 2011), SOL/INSOL uses UKCA's in-built dust scheme in 2 insoluble modes in the accumulation and coarse ranges (Jones et al., 2022). The dust scheme roughly follows Mann et al. (2010), where CLASSIC's 6-bin dust emissions are mapped to the 2 lognormal modes according to Jones et al. (2021), wherein bin 2 + 1/2 Bin 3 is emitted to the accumulation mode, and 1/2 Bin 3 + Bin 4 + Bin 5 are emitted to the coarse mode (noting that bins 1 (< 0.2 μm) and 6 (> 20 μm) of the CLASSIC dust scheme are not included in UKCA).

https://doi.org/10.5194/egusphere-2026-4611
Preprint. Discussion started: 9 November 2026
© Author(s) 2026. CC BY 4.0 License.

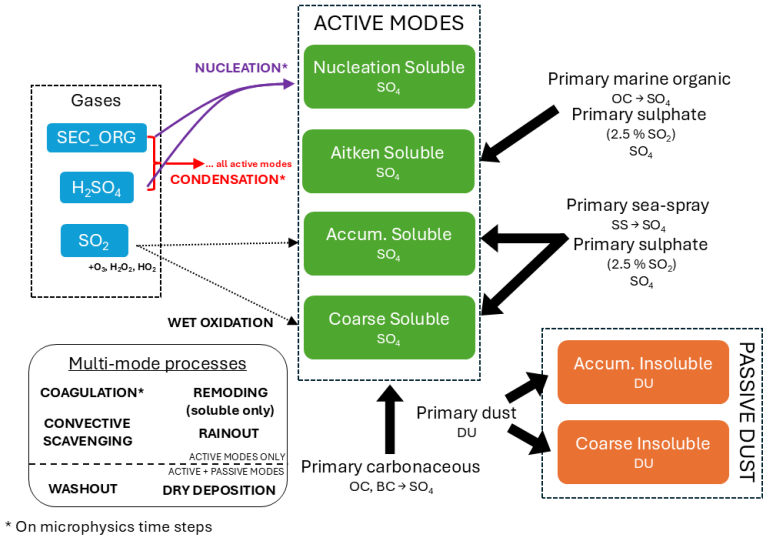

Figure 1. SOL/INSOL active and passive modes, alongisde the processes employed as described in section 2.3. Convective Scavenging only available when convection is parameterised.

Even conventional parametrised model setups may include a large number of tracers, which increase computational expense. For example, the upcoming UK-ESM2 incorporates nitrate following Jones et al. (2021) and includes a three-mode dust configuration, resulting in a total of 34 tracers. In comparison, SOL/INSOL (fig 1) has just 12 tracers (number and mass for the 4 soluble and 2 insoluble modes), aiming to reduce associated memory and time costs. Using one mass tracer per aerosol mode means that aerosol is treated as an internally mixed composition within the modal aerosol scheme (Mann et al., 2010). The particle's prescribed internal mixture is comprised of black carbon, organic matter, sulphate and sea salt. All soluble aerosol is treated like sulphate and insoluble treated like dust. Dust is treated as externally mixed and is passive in terms of chemistry: it remains insoluble throughout its atmospheric lifetime. As such it is not permitted to act as liquid cloud condensation nuclei (CCN) and thus be removed from the atmosphere by in-cloud scavenging or rainout (Jones et al., 2022), although it is scavenged by subcloud scavenging (section 2.3).

Rather than determining optical properties for the mixed aerosol composition online, as per conventional GA8/UKCA setups (e.g.: using UKCA RADAER (Willett et al., 2025)), SOL/INSOL further reduces computational cost by optionally utilising prescribed ancillary files of spectral single scattering albedo (SSA). If the option for prescribed SSA is not selected, SOL/INSOL uses the real refractive index for sulphate and the real refractive index for dust. An imaginary refractive index of zero is assumed for both soluble and insoluble components making them purely scattering. This method avoids the computational expense of determining and volume averaging the imaginary refractive index.

For this evaluation, all simulations use prescibed spectral SSA. Spectral SSA are derived by EasyAerosol (Voigt et al., 2014) with short-wave and long-wave extinction and absorption represented in 6 and 9 wavebands, respectively. Climatologies are comprised of pre-industrial, anthropogenic, and volcanic aerosol extinction contributions. The preindustrial extinction

https://doi.org/10.5194/egusphere-2026-4611
Preprint. Discussion started: 9 November 2026
© Author(s) 2026. CC BY 4.0 License.

profiles were derived from UM simulations from an N96 climate run. The anthropogenic files were generated internally from a FORTRAN package that was provided in Stevens et al. (2017). The volcanic files are a 3D copy of the CMIP6 volcanic ancillaries and originate from observations that were provided freely as part of CMIP6. The extinctions are then partitioned into their scattering and absorbing component contributions using the SSA. Figure C1 shows prescribed short-wave SSA for the 550 nm waveband, for July at a model level height of 955 meters, demonstrating a domain-average SSA of 0.93, decreasing to 0.86 over Greater London, UK, reflecting increased urban aerosol over the city.

2.2 Emissions

SOL/INSOL uses a combination of offline anthropogenic and online natural emissions.

Offline emissions for the nest are high resolution and from multiple sources. NetCDF ancillaries, including NAEI (both point sources and gridded sources over the UK at 1km resolution (Savage et al., 2013)), MEGAN-MACC (1 km^2, global) and EMEP (10 km^2, Europe) emissions datasets, are prepared for UKCA using the method employed by the Met Office operational air quality model (AQUM). This includes regridding raw emissions (ensuring mass conservation) to the UM model grid. NAEI point sources and EMEP Sector B_Industry are spread out across nine surrounding grid boxes and Dunkerque steel factory emissions are scaled by 0.1 (the operational scaling factor for 2019 datasets). At the time of writing, 2019 is the latest year for which emissions data are available. Emissions from 2019 have therefore been used throughout this study, and represent pre-COVID-19 pandemic conditions (that influenced emissions during 2020–2021). Emissions data sources are documented in section 6.7, Data Availability.

Aerosol and aerosol pre-cursors including black carbon (BC), organic matter (OM) and sulphur dioxide (SO_2) are classified according to their SNAP (Selected Nomenclature for sources of Air Pollution) sectors, of which there are eleven, allowing emissions from different sources to be treated differently for different sectors in the UKCA emissions scheme.

Emissions are provided as surface 2-D monthly totals and distributed temporily and vertically depending on sector. Given these offline emissions are provided as monthly means, seasonal patterns may be evident, but secular changes are not as well incorporated. Daily and weekly cycles are applied using SNAP-sector-specific hourly and daily scaling factors based on TNO (Netherlands Organisation for Applied Scientific Research) for the Monitoring Atmospheric Composition and Climate (MACC) project (Denier van der Gon et al., 2011). Vertical variation is applied as percentage contributions of SNAP-sector-specific emissions distributed over 6 fixed vertical model layers, as per Bieser et al. (2011)'s SMOKE model.

For BC and OM, fossil, biofuels and biogenic emissions are treated as fossil fuel with a modal diameter of 60 nm. The simplicity of this approach will be tested in the future by looking at model sensitivity to emissions. We also assume that 2.5% of SO_2 emissions are emitted as primary sulphate, as recommended for the AEROCOM global aerosol microphysics model intercomparison (Mann et al., 2010).

In terms of online natural emissions, sea salt and dust are represented in accumulation and coarse modes by diagnostic concentrations derived from wind-based parameterisations. Sea salt emissions follow the Gong-Monahan parameterisation (Gong, 2003) over the open ocean only. Dust emissions are as per Woodward et al. (2022) for the 6-bin CLASSIC dust scheme, where emissions are determined each time step based on Marticorena and Bergametti (1995), which calculates fluxes

https://doi.org/10.5194/egusphere-2026-4611
Preprint. Discussion started: 9 November 2026
© Author(s) 2026. CC BY 4.0 License.

over 9 horizontal and 6 vertical bins. The dry threshold friction velocity for each bin is taken from Bagnold (1941), and the effect of soil moisture on emissions is according to Fecan et al. (1999). Dust emissions are mapped to SOL/INSOL modes as per section 2.3. Sea-to-air flux of dimethyl sulfide (DMS, a gas-phase aerosol precursors (Neal et al., 2017)) is calculated as a function of its concentration in seawater and windspeed following Liss and Merlivat (1986) (Gordon et al., 2023) where the concentrations of DMS in seawater are prescribed from Kettle et al. (1999).

2.3 Aerosol processes

Aerosol processes (nucleation, condensation, wet oxidation) and multi-mode processes (coagulation, remoding, convective scavenging (GLM only), rainout (active modes), washout and dry deposition (active and passive modes)) are summarised in figure 1.

Boundary layer nucleation follows Metzger et al. (2010), where organic compounds together with sulfuric acid both initiate the nucleation process (with nucleation rates at 1.5 nm dry diameter being determined by the concentrations of H_2SO_4 and secondary organics) and drive early growth, leading to the formation of aerosol and - under the right conditions - growth into CCN. As per Jones et al. (2026), new particle formation in the upper troposphere and lower stratosphere is also from the binary homogeneous nucleation of H_2SO_4 and water following Vehkamäki et al. (2002).

Particle growth by condensation of H_2SO_4 and secondary organic vapours onto all aerosol modes follows first order uptake theory with corrections for molecular effects and limitations in interstitial mass transport (Mann et al. (2010), Jones et al. (2026)). Wet oxidation - where sulphate mass is produced by aqueous oxidation of SO_2 - is from two aqueous reactions detailed in Mann et al. (2010): the heterogeneous chemical conversion of S(IV) = $SO_2.H_2O$ + HSO_3^- + SO_3^{2-} to S(VI) following an effective Henry's law and production of S(VI) by aqueous oxidation of S(IV) by O_3, both calculated following Seinfeld and Pandis (1998). The dissolved sulphate mass produced by these two aqueous reactions is partitioned between the soluble accumulation and coarse modes according to the ratio of their respective number concentrations to their sum.

Particle growth by coagulation is described in detail in Mann et al. (2010) and includes intra- and inter-modal collisions (collisions of particles in the same and different modes, respectively) by calculating coagulation kernels following Seinfeld and Pandis (1998). For soluble modes, intra- and inter-modal coagulation with both larger soluble and insoluble modes is included, whereas for insoluble modes only inter-modal coagulation with larger soluble modes is included. Re-moding (also known as upward mode-merging) also follows Mann et al. (2010). Here particle number and mass are transferred between soluble modes when mean diameter exceeds the upper limit for the mode due to increase of size from condensation or coagulation. Per the default UKCA-mode setup, downward mode merging is not represented (Jones et al., 2022).

Removal by rainout - when aerosols act as CCN and form cloud droplets or ice crystals (which form from homogeneous freezing of droplets whose number is controlled by ccn availability, and can also form heterogeneously on the insoluble coarse) which grow and fall as precipitation (also know as nucleation or in-cloud scavenging) (Jones et al., 2022) - is as per Mann et al. (2010). Rainout is applied to the soluble accumulation and coarse modes only. Large-scale rain removes particles at a constant rate equivalent to 99.9% conversion of cloud water to rain over 6 hours. Insoluble-mode particles are scavenged only in cold environments when temperatures are below 258 K (Mulcahy et al., 2020).

https://doi.org/10.5194/egusphere-2026-4611
Preprint. Discussion started: 9 November 2026
© Author(s) 2026. CC BY 4.0 License.

Washout, the process by which falling hydrometeors irreversibly collect aerosol particles in their path as they descend through the atmosphere (also denoted below-cloud scavenging (BCS) or impaction scavenging (Jones et al., 2022)) is of particular importance for the wet deposition of insoluble materials such as dust, for which a distint two-moment impaction scheme has been developed. This uses rain rates for large-scale precipitation to drive the scavenging rate, based on look-up tables for collision efficiency between aerosols and raindrops (Mann et al., 2010). The scheme uses collision efficiencies representing the processes of Brownian diffusion, interception, inertial impaction, phoresis, electric charge, and rear-capture on aerosol capture. An extensive review of these microphysical pathways is in Jones et al. (2022), who provides an inexpensive BCS algorithm to calculate the BCS rate offline in the UKCA. Dry deposition and sedimentation follow the double-moment resistance type framework outlined by Mann et al. (2010), based on the parameterisation of Zhang et al (2001) which uses the method in the model of Slinn (1982).

2.4 Chemistry

The UKCA submodel permits chemistry schemes of varying complexity. In this report, we use the simpler offline-oxidants chemistry scheme, for which simulations are approximately twice as fast as those using the more complex StratTrop chemistry (Gordon et al., 2023). Here oxidant fields O_3, OH, NO_3, and HO_2 are provided as monthly-mean ancillary files, and only tropospheric aerosol precursor species H_2O_2, DMS, SO_2, sulphuric acid (H_2SO_4), $(CH_3)_2SO$, Monoterpene and secondary organics are retained as advected tracers (Walters et al., 2019). Scaling is applied to monthly means to mimic the diurnal cycle of OH and HO_2 (zero at night, cosine of zenith angle during the day), and to reduce NO_3 concentrations to zero during the day, as it photolyses readily. Hydrogen peroxide (H_2O_2) is highly soluble and therefore affected by wet deposition, hence this species is given a chemistry production and loss mechanism. As the source of H_2O_2 (HO_2) is not depleted, the H_2O_2 concentration is not allowed to exceed a limit provided by an offline ancillary file (Mulcahy et al., 2020). Chemistry for the offline oxidants is represented by the aerosol chemistry in the Newton-Raphson tropospheric chemistry solver (Esentürk et al., 2018). Note that nitrate processes as per Jones et al. (2021) are not included in SOL/INSOL due to the scheme's dependence on a more expensive chemistry scheme.

2.5 Lateral Boundary Conditions

A global model representative of the Met Office operational global forecasting system (MOGREPS-G) produces the fields necessary for the generation of lateral boundary conditions (LBCs) for the UKV. The ∼20 km grid spacing, 70 level GLM employs Global Atmosphere 8 (GA8) and Global Land 9 (GL9) science configurations, that represent the atmosphere–land–ocean–sea-ice interactions (Willett et al. (2025), in print) across 1280 x 960 latitude, longitude points.

The GA8GL9 configuration (Willett et al. (2025), in print) builds upon GA7GL7 (Walters et al., 2019) and introduces major updates to cloud processes that substantially improve cloud microphysics, precipitation behaviour, and cloud–radiation interactions. These include improved parametrisations for riming (increasing the amount of supercooled liquid water, resulting in more realistic mixed-phase clouds) and prognostic based entrainment (improving the spatial structure of convection, the vertical transport of moisture and precipitation rates). GA8 also includes the UKCA submodel, where for this study, size

https://doi.org/10.5194/egusphere-2026-4611
Preprint. Discussion started: 9 November 2026
© Author(s) 2026. CC BY 4.0 License.

distribution and composition of aerosol particles is represented using the SOL/INSOL aerosol scheme. GA8 has a 450 second (7.5 minute) timestep, with a chemistry timestep every 15 minutes, with 15 aerosol microphysics sub-timesteps. The GLM is initiated with zero spin up; global aerosol precursor fields are initialised using 12Z output from the ECMWF Copernicus Atmospheric Modelling Reanalysis project (CAMSRA, Inness et al. (2019)) and the fields to generate LBCs are provided at hourly intervals.

2.6 Aerosol precursor fields

CAMSRA includes a hybrid bulk-bin aerosol scheme comprising of hydrophilic and hydrophobic black carbon (BC) and organic matter (OM), sulphate (SO_4) in addition to dust and sea salt in 3 independent bins (see figure **??** for bin ranges). Aerosol is treated as being externally mixed and allows ageing of hydrophobic OM and BC to hydrophilic OM and BC (Inness et al. (2019), Bozzo et al. (2017). Nitrate aerosols are not included in the CAMSRA aerosol scheme which may cause an underestimation of total aerosol in regions where nitrate would be a significant component (Inness et al., 2019). A 12th tracer, SO_2, the gas phase precursor (Inness et al., 2019) is also available in CAMSRA, although we currently restrict our analysis to the aerosol phase only. Initialisation with the gas phase may be explored in future.

https://doi.org/10.5194/egusphere-2026-4611
Preprint. Discussion started: 9 November 2026
© Author(s) 2026. CC BY 4.0 License.

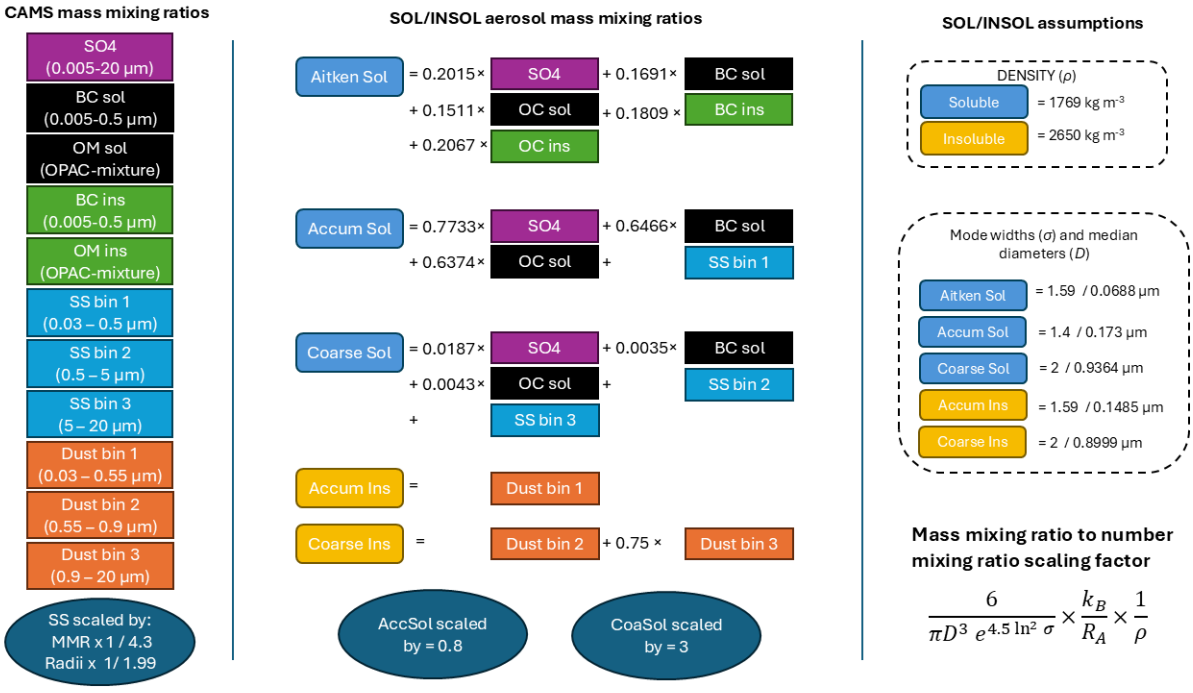

Figure 2. Left: CAMS Reanalysis aerosol speciation with bin size limits from Inness et al. (2019) and Bozzo et al. (2017), with mass mixing ratio and radius scaling factors to convert sea salt from 80% relative humidity to dry. Middle: Percentage species apportionment in to 5 SOL/INSOL modes along with the soluble accumulation and coarse modal scaling factors. Right: Equation to convert mass mixing ratios to number mixing ratio and its component definitions; density (Mann et al., 2010), modal widths and median diameters

.

CAMSRA SO_4, BC and OM bins straddle the entire width of the soluble modes for SOL/INSOL, hence the mass in these bins are apportioned to the different SOL/INSOL modes according to the mass mixing ratios given in figure 2. These constituent ratios are approximated using annual global mean tropospheric mass burdens of these components from a standard GA-AMIP (the Global Atmosphere - Atmospheric Model Intercomparison Project (Gates et al., 1999)) 20 year simulation. Broadly; calculating number and mass in each mode allows the ratios to be numerically determined, and omits any vertical dependency on the speciations by mode (for instance, smaller primary aerosol are emitted at the surface and then may grow as they are transported vertically). Note that as the Aitken insoluble mode is not included in SOL/INSOL, the hydrophilic BC and OM mass is added to the Aitken soluble mode. No CAMSRA mass is converted to SOL/INSOL's nucleation mode given the very small sizes and thus negligable impact.

Median diameters of SO_4, BC and OM are estimated from modal volume mean diameters from GA-AMIP over a range of heights from the surface to 4 km. These diameters are then used to translate 3D global CAMSRA mass mixing ratios to UKCA number mixing ratios using the equation in figure 2, where D is the median diameter (μm), k_b is the Boltzmann constant, R_A is

https://doi.org/10.5194/egusphere-2026-4611
Preprint. Discussion started: 9 November 2026
© Author(s) 2026. CC BY 4.0 License.

the specific gas constant for dry air and ρ is the particle density, set to 1769 and 2650 kg m^{-}3 for soluble and insoluble modes (Mann et al., 2010), respectively.

CAMSRA sea salt mixing ratios are provided at 80% relative humidity and transformed to dry matter using a reduction factor of 4.3 for the mixing ratio, and 1.99 for the radii of the sea salt bin limits (ECMWF (2023), Morcrette et al. (2009), Reddy et al. (2005)). The logarithmic distribution of the bins are used to derive the volume mean diameter to allow translation from sea salt mass to number concentration, as well as to derive the fraction of bin-3 mass aportioned to the target mode. For dust, a similar approach is taken whereby the volume mean diameter is inferred from a climate resolution GLM.

Initial UKV simulations suggested a consistent aerosol mass bias in comparison to that observed. We therefore employ empirical scaling factors of 0.8 and 3.0 to the soluble accumulation and coarse mode initial conditions to improve fidelity of the simulations. The significant correction applied to the coarse mode reflects its higher inherent uncertainty. In CAMS reanalysis, aerosol fields are constrained through data assimilation of aerosol optical depth (AOD, column-integrated light attenuation due to aerosol), typically measured at 550 nm. However, coarse-mode particles (e.g. sea salt) often have diameters significantly larger than this wavelength, making AOD at 550 nm relatively insensitive to the largest particles. As a result, the assimilation provides only indirect constraints on the coarse mode, and its representation relies more heavily on empirical corrections. These adjustments are therefore subject to ongoing tuning and refinement.

3 Observations

We employ a panoply of observations from the surface and throughout the atmospheric column, enabling comprehensive evaluation of SOL/INSOL throughout the boundary layer.

3.1 Surface and near surface $PM_{2.5}$

At surface level, the DEFRA-run Automated Urban and Rural Network (AURN) ground stations provide continuous hourly observations of $PM_{2.5}$, using Optical Particle Counters (OPC), which determine number and size of dried particulates using a light scattering technique, with conversion to mass concentration (save for one London site, which uses beta ray attenuation). AURN instruments are maintained to meet an uncertainty of $\leq$ 25%, although they often perform better in practice, achieving uncertainties closer to $\sim$ 10% (Department for Environment, Food and Rural Affairs, 2023). AURN sites range from rural/remote to kerbside locations, however, given the resolution of SOL/INSOL is best suited to modelling background and regional aerosol, away from strong, localised sources of pollution, here we consider only the rural, urban and suburban background AURN sites (Neal et al., 2014).

At (approx.) 7 meters above ground level in London (51.45087, -0.03749, approx. 30 meters elevation (Google LLC, 2023)), Manchester (53.4566, -2.2142, 43 meters) and Birmingham (52.45033, -1.93052, 140 meters), Integrated Research Observation System for Clean Air (OSCA) masts, instrumented to measure pollutants as part of the UK Clean Air Programme (Watson et al. (2023), UKRI (2021)), provide $PM_{2.5}$ observations also derived from OPC. London and Birmingham OSCA data are provided at 15 and 1 minute intervals, respectively. Manchester OSCA data are derived from a sampling frequency of 10 seconds

https://doi.org/10.5194/egusphere-2026-4611
Preprint. Discussion started: 9 November 2026
© Author(s) 2026. CC BY 4.0 License.

and averaged over one minute. Where shown, all OSCA data is further averaged over MOASA transect times (see following section). Additionally, observed aerosol particle size distributions (PSD) are available from the Manchester OSCA mast. These are used to further scrutinize the agreement between airborne and predicted size distributions in section 5.2.1.

3.2 Boundary layer $PM_{2.5}$

At altitudes from around 300 m and into the free troposphere, the instrumented Cessna-421 Met Office Atmospheric Survey Aircraft (MOASA) provides quality-assured, three-dimensional observations of common pollutants, including $PM_{2.5}$. As part of CAP, a total of 63 flight sorties were flown between July 2019 and April 2022, comprising over 150 hours of atmospheric sampling over the south of the UK across a range of sortie types, including city scale, coastal transition and high-density plume mapping. These data are openly available from the Centre for Environmental Data Archive (CEDA, DOI: https: //doi.org/10.5285/0aa1ec0cf18e4065bdae8ae39260fe7d, Mynard et al. (2023)). Here, $PM_{2.5}$ is again derived from an OPC. These size data are calibrated, corrected for index of refraction and used to derive mass distributions by assuming a fixed particle density of 1640 kg m^{-3}. $PM_{2.5}$ is associated with an uncertainty of 20.4% as detailed in Mynard et al. (2023). This paper employs MCAP city scale sorties, which observed emissions and dispersion of pollutants above heavily populated, commercial and industrial regions. These flights typically involved circumnavigational orbits or box patterns over the cities at altitudes ranging from approximately 0.3 to 0.9 km, included runs upwind and downwind of the city and overpassed the OSCA mast sites where possible. Aircraft data is sampled at 1 Hz at around 85 meters per second true air speed and averaged over 10 second intervals to minimise variability from instrument noise and precision. Only data from straight and level runs (SLRs; flight transects at approximate constant altitude and velocity) of at least 3 min duration are included.

Airborne aerosol distributions are also derived from the OPC size and number measurements, according to Mynard et al. (2023), using calibrated, index of refraction corrected data. Observed number and volume PSD are normalised by bin width in log space. An aerosol distribution model was created as the sum of two lognormals and fit to the OSCA and airborne distributions to reduce the impact of Mie resonances during derivation of particle size (Mynard et al., 2023). See Mynard et al. (2023) for a full description of the flight campaign, data and measurement techniques.

3.3 Total column AOD

Finally, satellite observed aerosol optical depth serves as a proxy for aerosol loading throughout the atmosphere and as such is commonly used to compare observations of aerosol to modelled aerosol loadings. Here, the 10 x 10 km NASA Moderate Resolution Imaging Spectroradiometer (MODIS) MOD04_L2, 550 nm AOD product is selected (Wei et al., 2020) to augment the aircraft observations and the comparitively sparsely horizontally distributed ground network.

The MOD04_L2 AOD product for the case studies are acquired as HDF files from NASA Earthdata. Retrievals generated using the Merged Dark Target/Deep Blue AOD algorithm are selected to provide optimal coverage above both bright and dark surfaces. Level 2+ quality assurance flags, offset and scaling factors (as provided in the HDF metadata) are applied to the retrievals.

https://doi.org/10.5194/egusphere-2026-4611
Preprint. Discussion started: 9 November 2026
© Author(s) 2026. CC BY 4.0 License.

Zone	Product	Instrument/observation method	Source
Surface	AURN	Primarily Palas Fine Dust Operating System (FIDAS) light scattering spectrometer with built in conversion to mass	DEFRA
Near surface	OSCA	Palas Fine Dust Operating System (FIDAS) light scattering spectrometer with built in conversion to mass	SPF Clean Air, CEDA collection, Watson et al. (2023)
Boundary layer	MOASA Clean Air (MCAP) database	Airborne Portible Optical Particle counter (POPS) with conversion to mass concentration using an interative method (see Mynard et al. (2023))	SPF Clean Air
Total column	MODIS	Satellite based imaging spectroradiometer, with Merged Dark Target/Deep Blue AOD at 10km x 10 km	NASA Earthdata

Table 1. Observations summary

Retrievals of AODs from MODIS are in good agreement with independent groundbased AERONET measurements, with canonical errors reported to be $\pm$ 0.05 $\pm$ 0.2 x AOD over land (Reddy et al. (2005), Chu et al. (2002)).

3.4 Observation coherence

Mynard et al. (2023) showed good agreement (r^2 = 0.90) between airborne and ground-based $PM_{2.5}$, by comparing average airborne $PM_{2.5}$ within a 12km radius of a ground-site, against the average for that ground-site, for the duration of the flight, for all London flights in the MCAP dataset. Given the applicability to the case studies evaluated here, this analysis is extended to the Manchester and Birmingham regions. The results are shown in Fig 3, alongside the London figure from Mynard et al. (2023) for completion. These confirm airborne and ground-based observations also agree well for Birmingham (r^2 = 0.96) and Manchester (r^2 = 0.08), whose results - albeit with near-zero R^2 likely due to comparitively low aerosol loadings - straddle the 1-2-1 line. This observational coherence across all sites suggest observations were made in a well-mixed atmosphere, with little gradient in mass concentration in the lower atmosphere (up to the aircraft altitude). Figure 3 also demonstrates that ground, mast and airborne observations of $PM_{2.5}$ are comparable, regardless of observation technique employed. The strong similarity between mast-based and airborne-observed PSDs (fig 10, section 5.2.1) lends further confidence to the methods used to derivate

https://doi.org/10.5194/egusphere-2026-4611
Preprint. Discussion started: 9 November 2026
© Author(s) 2026. CC BY 4.0 License.

the size distributions and subsequently mass concentration, and also suggests the lower atmosphere behaves in a physically consistent manner with little vertical variation in aerosol number and size. These consistencies support the use of the more spatially abundant airborne observations to augment ground-based observations in this model evaluation.

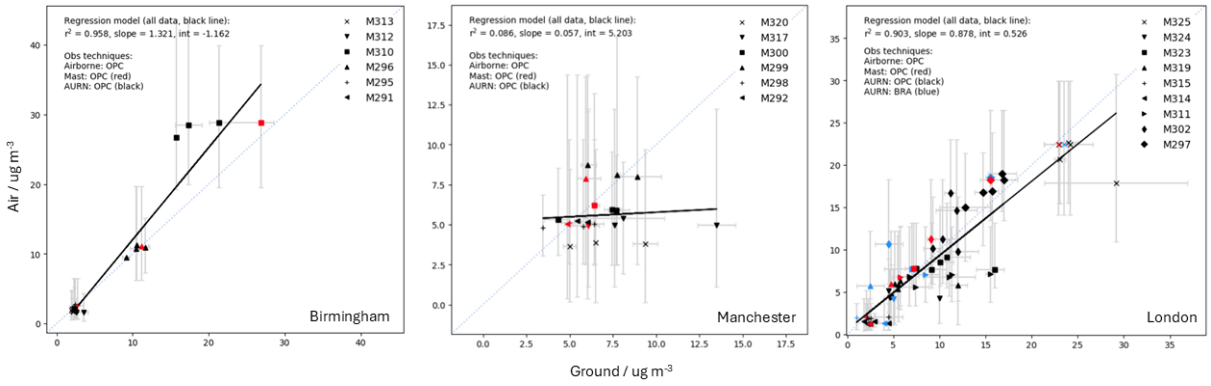

Figure 3. Average airborne observations of $PM_{2.5}$ within a 12km radius of ground site against local ground-site average $PM_{2.5}$ for the duration of the flight, for Birmingham, Manchester and London. Comparisons against OSCA mast data are shown in red and against AURN ground sites in black. Blue markers identify those AURN sites that employ beta ray attenuation (denoted 'BRA' in the legend) technique, black employs an optical particle counter with conversion to mass technique (denoted as 'OPC'). Linear regression between airborne and ground- and mast-based data is shown in black. Error bars (grey) show the range of data; the 1–2–1 line, representative of a perfect linear relationship, is shown as a dotted grey line.

To compare 1.5 km gridded, 6-hourly output time averaged model data with the spatially and temporally high resolution airborne data, the model grids nearest the aircraft measurement locations (latitude, longitude, and altitude) and times are extracted from the 4D field. From hereonin, any comparison of model data with aircraft data can be assumed to be co-located. Similarily, for the surface and near surface observations, data is averaged over the flight duration and the model grids nearest the measurement locations (latitude, longitude) are used.

MODIS typically captures satellite images over the UK between 10:00 and 14:00 UTC each day (at 5 minute intervals), which is roughly concurrent with the model data at 13:00, and the MOASA flight times (which generally took place between 11:00 and 15:00). No downscaling has been applied to the MODIS data; to avoid mis-matches from sub-grid variability, MOD04_L2 10 km swath data is regridded on to a 0.1 x 0.1 grid (approx. 10.11km) and compared to the average model data in each satellite grid box. Satellite coverage over the UK was varied across the case dates, with only five cases (see appendix G) providing sufficient AOD retrievals for meaningful comparison (e.g.: due to cloud cover). The availability of satellite data was therefore an important consideration in the selection of a single case study for more detailed analysis.

https://doi.org/10.5194/egusphere-2026-4611
Preprint. Discussion started: 9 November 2026
© Author(s) 2026. CC BY 4.0 License.

4 Case studies

We select 15th June 2021 for in-depth evaluation of SOL/INSOL due to the comprehensive suite of observations available on this date. These include MCAP flight M293 - which this case study will be known as forthwith - which measured $PM_{2.5}$ over the Greater Manchester region from 10:18 to 11:09 (310 data points) at altitudes from 358 to 1094 meters. The airborne observations are complemented by near-surface measurements from the Manchester OSCA mast, which includes PSD, and data from 78 surface AURN sites across the UK; 6 of which are in the North West and Merseyside AURN region (which encompasses Greater Manchester) and 2 of which are within 12 km of M293 aircraft data. There is also marginal availability of MODIS retrievals to allow evaluation of predicted AOD.

Prevailing weather conditions for M293 are summarised in figure 4 showing the Met Office synoptic chart alongside satellite-derived cloud cover and rainfall at 12:00 UTC on 15th June 2021. A low-pressure system situated to the west of the UK produced generally unsettled and cooler conditions across northern parts of the country, characterised by extensive cloud cover and periods of rain. In contrast, southern regions were predominantly influenced by high pressure extending from the east, resulting in relatively light winds, thin and broken cloud, and warmer conditions, with maximum temperatures reaching 26.6 °C in London (Met Office National Climate Information Centre et al., 2021).

The M293 case study was executed in several model configurations to enable a comprehensive assessment of SOL/INSOL. The 'control' suite, run with 1 hour lead time (giving a snap shot of 13:00 on 15th June 2021) and a full compliment of CAMSRA initial conditions (ICs), is used to assess the performance of SOL/INSOL in comparison to observations on a national and regional scale. In the following evaluation, the model is assumed to maintain this configuration throughout, unless explicitly stated otherwise. For example, sensitivity experiments were carried out by modifying individual CAMSRA aerosol species in suites labelled ST$species$ (sec. 5.3), and the model's forecasting skill was evaluated using suites denoted Fxhh, where 'hh' represents the extended forecast lead times in hours (sec. 5.4). A summary of all simulations included in this study is shown in Table 2.

ID (suite ID)	Simulation date + lead time	Initial conditions
Control (u-du900)	20210615T1200Z + 01 hrs	CAMSRA
ST_{SS} (u-dv914)	20210615T1200Z + 01 hrs	CAMSRA - zero seasalt
ST_{OM} (u-dv915)	20210615T1200Z + 01 hrs	CAMSRA - zero organic matter
ST_{BC} (u-dv916)	20210615T1200Z + 01 hrs	CAMSRA - zero black carbon
ST_{SU} (u-dv918)	20210615T1200Z + 01 hrs	CAMSRA - zero suphates
Fx_{13} (u-du900)	20210615T0000Z + 13 hrs	CAMSRA
Fx_{25} (u-du900)	20210614T1200Z + 25 hrs	CAMSRA
Fx_{37} (u-du900)	20210614T0000Z + 37 hrs	CAMSRA

Table 2. Summary of simulations used in this report. ST = Sensitivity test, SS = sea salt, OM = Organic matter, BC = Black carbon, SU=Suphates. Fx = Forecast test

https://doi.org/10.5194/egusphere-2026-4611
Preprint. Discussion started: 9 November 2026
© Author(s) 2026. CC BY 4.0 License.

An additional 30 cases, concident with MCAP city survey research flights, are used to provide further statistical support for evaluating the SOL/INSOL aerosol scheme. Cases are divided into regions: Manchester, Birmingham and London. Case dates, aircraft flight times and altitudes, and number of available AURN sites for each case are summarised in tables A2, A3 and A4. All flight cases were situated around heavily populated, commercial and industrial regions. In terms of meteorology, conditions for the additional cases are representative of both the general background environment and elevated pollution events. Further details on these MCAP flight sorties can be found Mynard et al. (2023). Note that the simulations differ from case to case in three ways: initial conditions from CAMSRA, the emissions and meteorology.

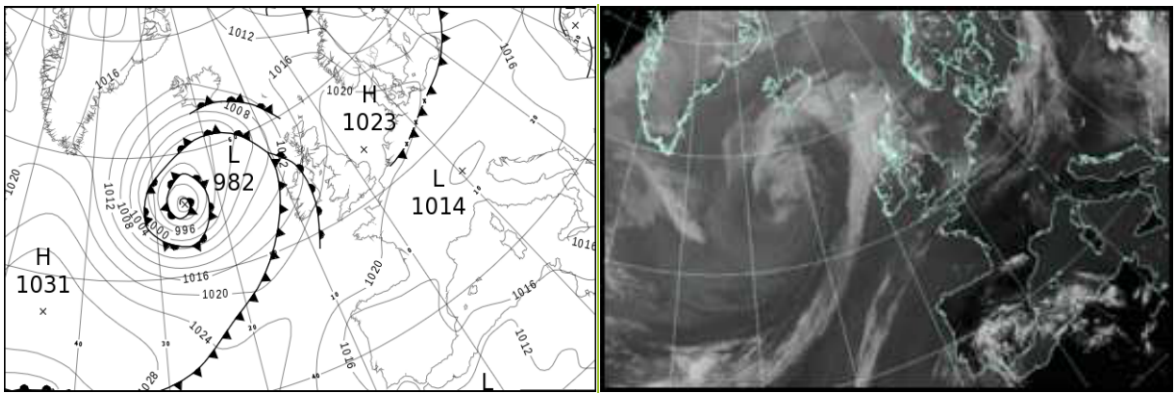

Figure 4. North Atlantic and Europe analysis charts and satellite images for 1200 UTC on 15th June 2021 (M293). copyright Met Office and EUMETSAT (European Organisation for the Exploitation of Meteorological Satellites. These show infra-red images from the geostationary MSG satellite.

5 Results

In this section, we first examine nationwide SOLINSOL $PM_{2.5}$ (section 5.1), comparing model outputs with ground-based AURN $PM_{2.5}$ observations and by comparing modelled AOD with satellite-derived estimates (section 5.1.1). Next, we investigate the regional impact of SOLINSOL on $PM_{2.5}$ (section 5.2), incorporating airborne observations and analysing microphysical properties through particle size distributions (section 5.2.1). Section 5.3 examines the contributions of individual CAMSRA components to $PM_{2.5}$, and finally, section 5.4 assesses the forecast skill of the model.

https://doi.org/10.5194/egusphere-2026-4611
Preprint. Discussion started: 9 November 2026
© Author(s) 2026. CC BY 4.0 License.

5.1 Nationwide (UK)

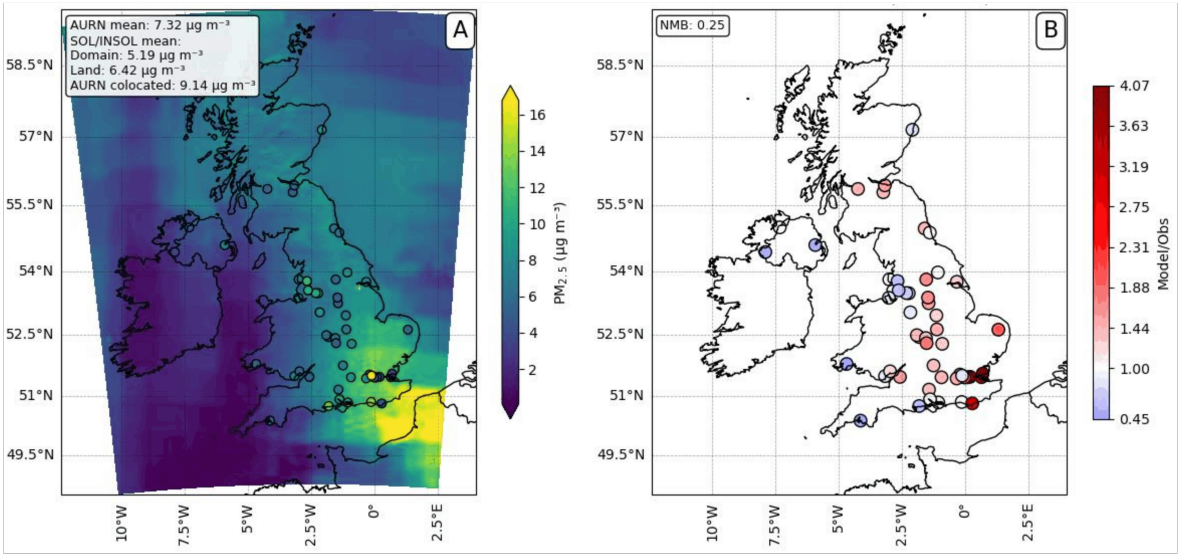

Figure 5. Panel A: Surface level SOL/INSOL predicted $PM_{2.5}$ over the UK for 13:00 on 15th June 2021, overlaid with mean urban background AURN $PM_{2.5}$ (circles) from 12:00 - 14:00. The colorscale range spans the 1st to 99th percentiles of the data from both datasets. The legend provides mean UK-wide AURN alongside mean SOL/INSOL over the UKV domain, over land only and co-located with the AURN sites. Panel B: SOL/INSOL co-located $PM_{2.5}$ divided by AURN $PM_{2.5}$ mean, where a score of 1 (white) indicates agreement between datasets, >1 (red) indicates model over-prediction and <1 (blue) indicates model underprediction. The Normalised Mean Bias (equation 1) is shown in the top left.

Figure 5 depicts the UK domain, showing predicted surface-level SOL/INSOL $PM_{2.5}$ (from the control suite) with observed $PM_{2.5}$ overlaid (panel A), and the spatial differences between the two datasets (panel B).

Predicted surface $PM_{2.5}$ over the UKV domain is 5.19 μg m^{-3} and slightly higher over the land mass at 6.42 μg m^{-3}. A large area of elevated aerosol concentrations are seen over the channel in the south-east, peaking around 16 μg m^{-3}, with some much smaller, isolated peaks visible in east side of the country. Ships tracks are visible in the channel. Mean predicted $PM_{2.5}$ co-located with background AURN surface observation sites is 9.14 μg m^{-3}. Mean $PM_{2.5}$ at the observation sites is slightly lower at 7.32 μg m^{-3}. Isolated areas of elevated $PM_{2.5}$ are observed at familiar pollution hotpots such as the Westminster AURN site in London in the south-east (mean: 17.33 μg m^{-3}).

https://doi.org/10.5194/egusphere-2026-4611
Preprint. Discussion started: 9 November 2026
© Author(s) 2026. CC BY 4.0 License.

Panel B demonstrates reasonable agreement between predicted and observed surface $PM_{2.5}$ across the UK, with most site ratios between 0.5 - 1.5, indicating agreement within ±50%. For M293, the model generally over-predicts as evidenced by predominantly red sites. A cluster of moderate (3- to 4-fold) overpreditions are evident across the south-east, suggesting the model may over predict aerosol concentration in the plume.

Model skill is quantified in terms of the normalised mean bias, NMB, shown in equation 1, where mean values are used to reduce the influence of sample size and outliers. The NMB for M293 is 25%, indicating moderate overall agreement, with a tendency towards over-prediction for this case study.

$$NMB = \frac{\bar{M} - \bar{O}}{\bar{O}} \tag{1}$$

To examine if M293 is representative of general model performance, this analysis is extended to include all city survey research flights from MCAP. The results are summarised in table 3 which shows the grand medians (the median of all case study means, where the median is used to reduce the influence of outliers and skewed cases) across 31 cases for a range of groupings (less and greater than 10 $PM_{2.5}$, and seasonal groups). Results for these groupings, alongside case details, mean predicted $PM_{2.5}$ over the UKV domain, over land, co-located with AURN sites and observed $PM_{2.5}$, the associated NMB and grand medians are presented in full in table A1.

Table 3. Grand median (the median over 31 case study means) surface SOL/INSOL predicted $PM_{2.5}$ across the UKV domain, over the UK land only and co-located (CL) with UK-wide AURN sites, alongside mean observed UK-wide AURN $PM_{2.5}$ (over 1 hour either side of model time of 13:00). The final column shows the median NMB for model AURN-CL against AURN $PM_{2.5}$. Each row shows grand medians categorised as follows: over all cases ("MEDIAN"), those cases when AURN observed $PM_{2.5}$ >= 10 μg m^{-3} ("AURN OVER 10"), when AURN observed $PM_{2.5}$ < 10 μg m^{-3} ("UNDER AURN 10"), and for seasonal splits (where "SUMMER" = JJA, "AUTUMN" = SON, "WINTER" = DJF and "SPRING" = MAM). The numbers in brackets in the row header indicates how many cases were used to calculate each respective median (noting the Autumn median is absent due to just one case falling in this category). The full table detailing the locations, dates, number of datapoints, means and NMB for individual cases is in table A1.

Grand medians	Model: mean over domain	Model: mean over land	Model: mean AURN-CL	Mean UK-wide AURN	NMB
MEDIAN (31)	3.98	3.87	5.97	6.64	-0.13
AURN OVER 10 (5)	8.17	9.29	13.19	13.76	-0.10
AURN UNDER 10 (26)	3.72	3.45	5.18	5.90	-0.16
SUMMER (11)	5.19	5.37	8.64	6.65	0.02
AUTUMN (1)	-	-	-	-	-
WINTER (12)	3.06	2.67	4.18	5.59	-0.22
SPRING (7)	6.58	5.20	5.97	8.02	-0.22

The median model over the UKV domain is marginally higher than that over the land, which is unexpected due to proximity to land based emissions. Median colocated modelled and observed $PM_{2.5}$ are comparable, at 5.97 and 6.64 μg m^{-3}, respectively which is reflected in a modest model underprediction (median NMB) of -13% compared to observations. The bias reduces to -10% for cases with mean observed $PM_{2.5}$ > 10 μg m^{-3} (over 5 cases) and to +2% during summer (11 cases). It is more negative in spring and winter, reaching -22% across 7 and 12 cases, respectively. Overall, the NMB varies substantially across the 31 cases, ranging from a maximum underprediction of -47% (case M315) to a maximum overprediction of 88%

https://doi.org/10.5194/egusphere-2026-4611
Preprint. Discussion started: 9 November 2026
© Author(s) 2026. CC BY 4.0 License.

(case M302). Regardless, as shown in figure 6, generally predicted co-located and observed $PM_{2.5}$ correlate quite well (Pearson correlation coefficient, r = 0.83 and corresponding R^2 = 0.70) with higher variability seen where $PM_{2.5}$ is observed to be greater than 10 μg m^{-3} (r = 0.60, R^2 = 0.36). In this figure, the x-error reflects the temporal variability in the observations over the 3-hour averaging period, while the y-error represents the spatial variability in the model across neighbouring grid cells; in most cases, both uncertainties overlap the 1:1 line.

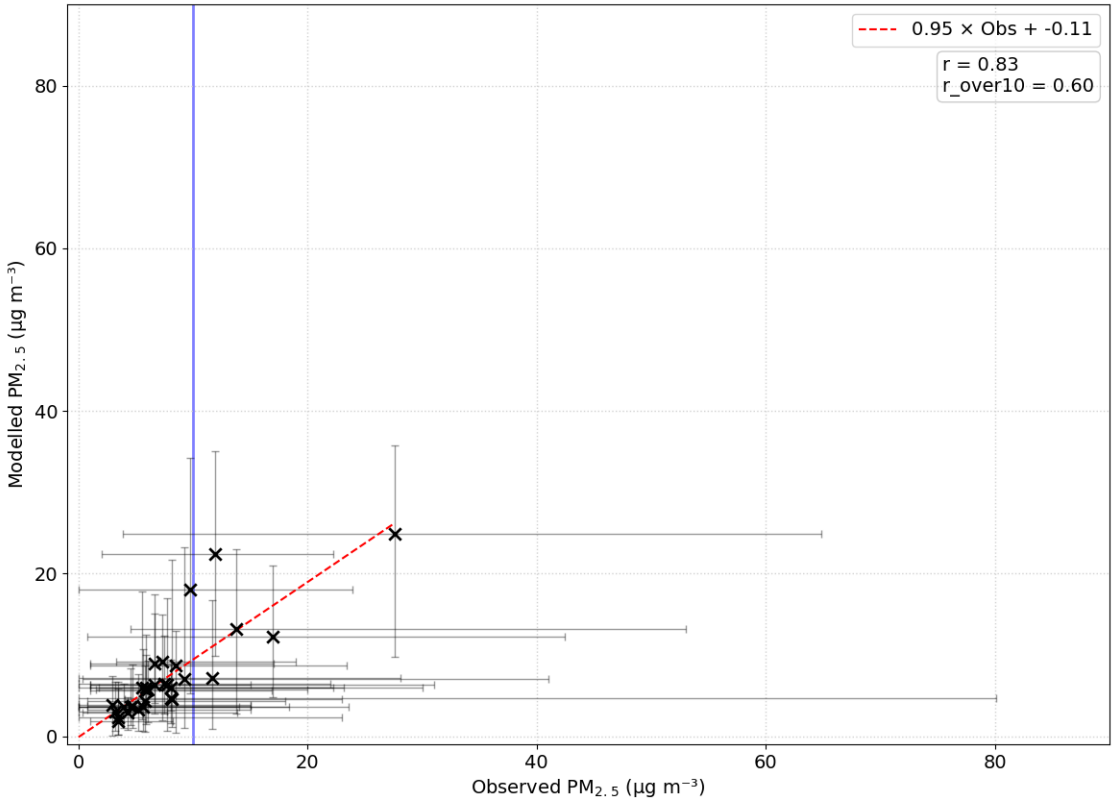

Figure 6. Mean AURN-co-located predicted $PM_{2.5}$ against mean AURN observed $PM_{2.5}$ for 31 cases detailed in table A1 and summarised in table 3. The observation error shows the minimum and maximum $PM_{2.5}$ across the 3 hours of data. The model error is the range across the eight grid cells adjoining the colocated grid cell. Line of best fit is shown (red, dashed) alongside the Pearson correlation coefficient (r). Also shown is the correlation coefficient for those cases where observed $PM_{2.5} \geq 10$ μg m^{-3} (r_over10, for cases to the right of the blue vertical line)

https://doi.org/10.5194/egusphere-2026-4611
Preprint. Discussion started: 9 November 2026
© Author(s) 2026. CC BY 4.0 License.

5.1.1 Aerosol optical depth

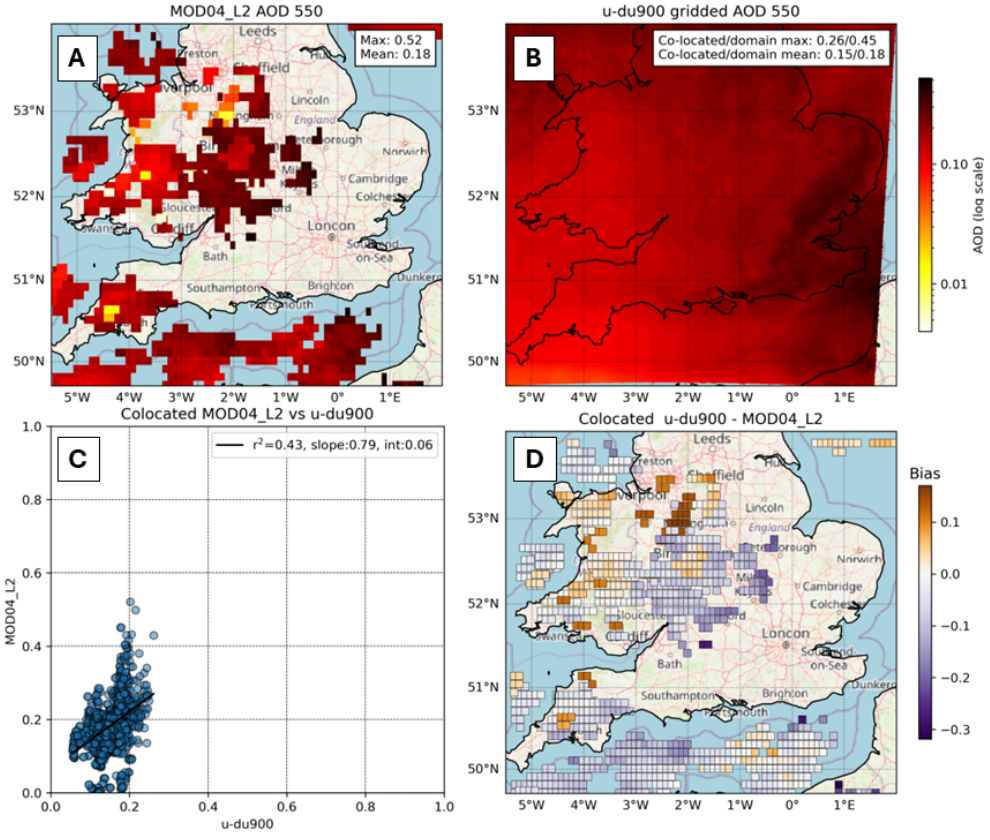

Figure 7. Panel A: MODIS 550nm aerosol optical depth (AOD) for satellite overpass times of 10:50, 10:55 and 12:30 on 15th June 2021. B: SOL/INSOL predicted 550 nm AOD at 13:00 15th June 2021, from CONTROL suite (u-du900, see table 2). C: co-located MODIS against SOL/INSOL AOD. D: mapped difference (SOL/INSOL - MODIS) of co-located AOD over southern UK where blue indicates a model underprediction, orange indicates an overprediction.

To augment the limited spatial coverage of ground-based observations in this study (which leave large regions — including Scotland, Wales, southwest England, and eastern England — sparsely monitored) we incorporate high horizontal resolution satellite observations. Figure 7 presents observed AOD from the MODIS satellite (panel A) alongside predicted SOL/INSOL aerosol optical depth (AOD, Aitken, accumulation and coarse mode total column AOD at 550 nm, panel B) for case M293. For this case, we see SOL/INSOL predicts similar mean AOD over the domain and colocated with the satellite (predicted colocated=0.15, predicted domain=0.18, observed=0.18) but maximum values are not as well represented given predicted maximum AOD (0.26) is half of that observed (0.52).

https://doi.org/10.5194/egusphere-2026-4611
Preprint. Discussion started: 9 November 2026
© Author(s) 2026. CC BY 4.0 License.

Given the limited satellite coverage for this case, other MCAP cases with reasonable satellite coverage (M300, M302, M325 and M292, see figure G1) are considered. These 4 additional cases show predicted co-located mean and maximum AOD are approximately a factor of two lower than observed.

R^2, the correlation between predicted and observed AOD (panel C), ranges from 0.43 (case M293, figure 7) to 0.84 across all 5 cases, and yield a mean R^2 of 0.64. Cases with higher AOD yield higher R^2. Figure G1 - notably case M325 with substantial satellite coverage - demonstrates that SOL/INSOL effectively reproduces the AOD patterns observed by MODIS, including broad country-scale gradients and mesoscale features. Mapped differences in panel D - notably for cases M293 and M294 - show the negative bias (blue) is not uniform over the domain and varies by location.

To further examine discrepancies in model bias across different locations, together with the nationwide negative bias identified above, the next section takes a regional approach, evaluating model performance over a specific area which may be impacted by local emissions and processes.

5.2 Regional insights

Having considered the nationwide picture of $PM_{2.5}$ predictions in SOL/INSOL, we now move to regional insights. Figures 8 and 9 show predicted and observed $PM_{2.5}$ in the vertical and horizontal planes, respectively, for M293 over the Greater Manchester region. As discussed in section 3.4, we see good coherence between airborne (red circles), surface and mast based observations (orange triangles, black star), suggesting a well-mixed boundary layer. Co-located model column $PM_{2.5}$ (blue lines) captures this mixing well, showing little variation in the vertical with the exception of a small reduction at the lowest model level.

https://doi.org/10.5194/egusphere-2026-4611
Preprint. Discussion started: 9 November 2026
© Author(s) 2026. CC BY 4.0 License.

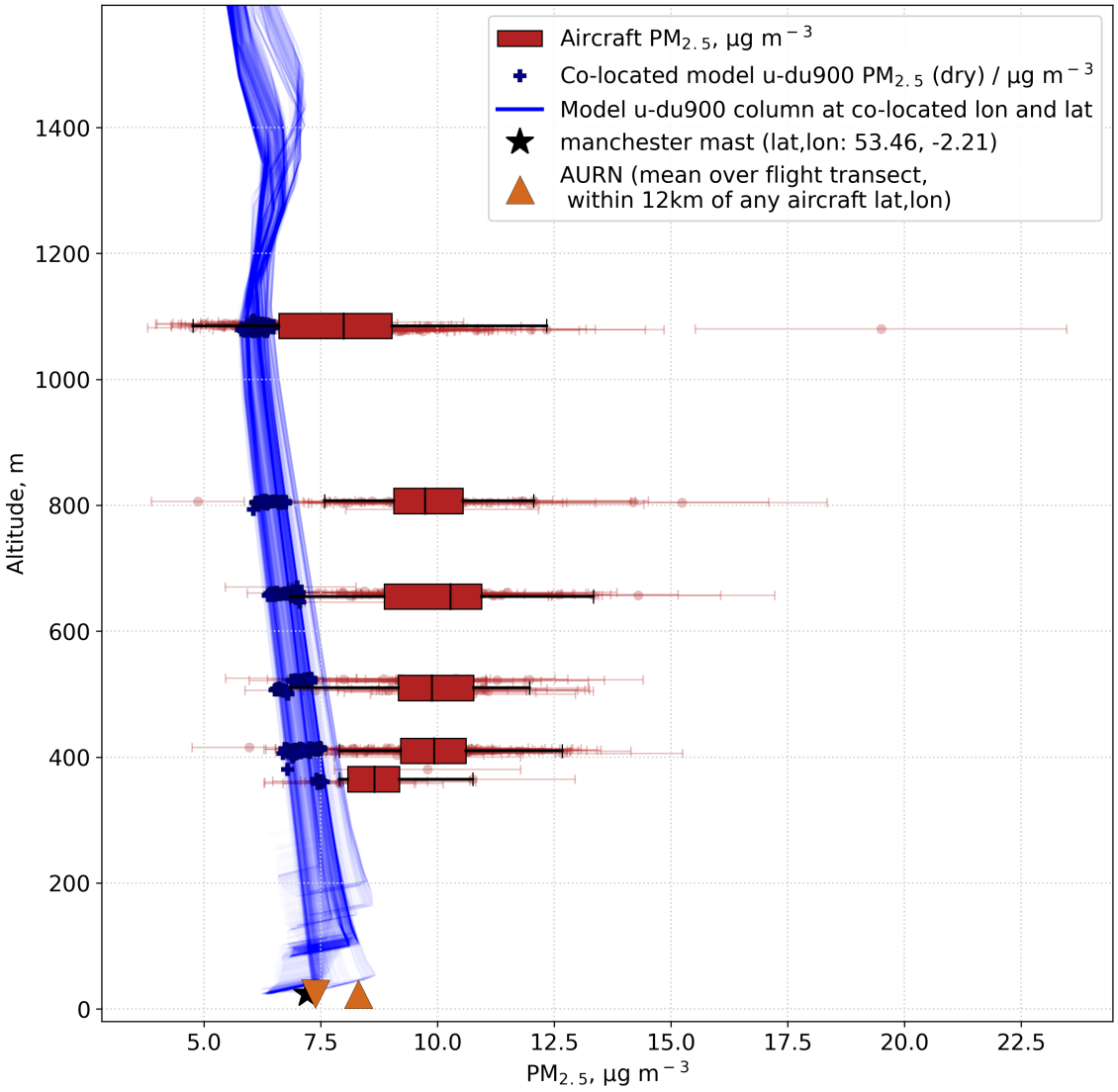

Figure 8. Profile of $PM_{2.5}$ from 10:18 to 11:10 for M293 on 15th June 2021. Aircraft $PM_{2.5}$ is shown in red (where boxes show the 25th to 75th percentiles) with data with errorbars underlaid to show outliers and measurement uncertainty (20.4 %). Control suite u-du900 colocated with aircraft latitude and longitude (columns) is shown in blue, and control suite colocated with the aircraft as dark blue crosses. Closer to ground level, OSCA mast $PM_{2.5}$ is shown as a black star with AURN $PM_{2.5}$ represented by orange shapes.

Predicted and observed $PM_{2.5}$ show near alignment throughout the atmospheric column, where the lower range of airborne observations overlap with the model. Agreement strengthens in the upper level run (1100 m), evident in a greater overlap between model and observed $PM_{2.5}$. Variation and uncertainty in airborne data is comparitively large, due to measurement uncertainties and sub-grid scale variability which may not be represented by the model (Mynard et al., 2023).

https://doi.org/10.5194/egusphere-2026-4611
Preprint. Discussion started: 9 November 2026
© Author(s) 2026. CC BY 4.0 License.

The upper level run is shown in the south-east quadrant of the flight track in figure 9, panel A, as the area with the lowest airborne concentrations, around $\sim$6 μg m^{-3}. This concentration doubles towards the north-west quadrant (the area which incorporates all runs below 1000 m in figure 8). Although the co-located model, panel B, captures some of this horizontal gradient, it does so to a lesser magnitude (a $\sim$2 μg m^{-3} increase from south-east to north-west).

Mean aircraft-colocated model $PM_{2.5}$ is 6.64 μg m^{-3}, which is compared to an airborne mean of 9.21 μg m^{-3} to yield a regional model-airborne bias (NMB) of –28% for M293. Extending to the 7 cases in the Manchester region (see A3 and figure A2) shows this model-aircraft bias is varied in sign and magnitude across the cases, and yields a median bias of -5% (NMB 1 in table A3). The median model-aircraft bias across the London (table A4, figure A3) and Birmingham (table A2, figure A1) regions are -29% and -1%, respectively.

The regional model-ground bias for M293 is substantially smaller at -7%, indicating an overall higher bias aloft (with the exception of the very upper level) for this case. Again extending this analysis to all Manchester cases, we see a higher bias aloft for 5 of 7 case studies in the region. This is contrary to the grand-median model-airborne (5%) bias which is lower than the median model-ground bias (14%) for this region. A higher bias aloft is also seen in 11 of 17 London cases which is represented by a median model-airborne bias of 29% and zero median model-ground bias. For the Birmingham region, only 2 of 7 cases show a higher bias aloft (table A2), reflected by a median model-airborne bias of 1% and a median model-ground bias of 9% indicating surface processes may not be as well captured in this region.

https://doi.org/10.5194/egusphere-2026-4611
Preprint. Discussion started: 9 November 2026
© Author(s) 2026. CC BY 4.0 License.

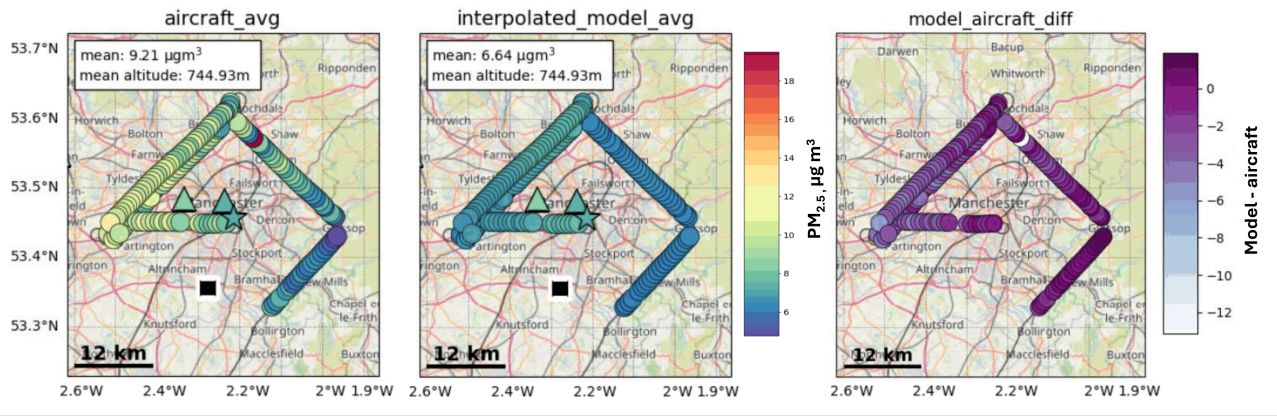

Figure 9. $PM_{2.5}$ over Manchester during flight M293 on 15th June 2021 (left) alongside co-located predicted $PM_{2.5}$ from control suite (u-du900, middle). Triangles and the star represent ground and mast based observations. The black square is Manchester airport. The right image shows the difference (model - aircraft) over the flight track.

5.2.1 Size distributions

To better understand the drivers of regional underprediction in case M293, we examine the microphysical processes that control mass concentration. An advantage of using the Manchester OSCA mast data is the availability of discrete aerosol number and sizing measurements. This enables a unique analytical opportunity to assess predicted PSD both at the surface and at higher altitudes. Observed and predicted number and volume PSD for M293 on 15th June 2021 are shown in figure 10. Airborne data (red) are averaged over 6 straight and level runs from 14:02:12 to 14:39:24 at altitudes from 400 to 1100 meters (as shown in figure 8). OSCA PSD (green) are averaged over the aircraft transect times.

Predicted number and volume PSD were derived by first linearly interpolating modelled diameter and number for soluble Aitken, accumulation and coarse modes over the times and position of the aircraft. Given the UK is not generally subjected to dust clouds (being more impacted by localised anthropogenic aerosol sources) the dust contribution to $PM_{2.5}$ over the UK is deemed negligable (as evidenced by figure B1 in appendix B from the case date) and the insoluble contribution to the distributions are omitted to save the computational expense of interpolation. For each soluble mode, mean co-located diameter and number over the transect are used to derive number distributions using equation (2) and volume distributions

https://doi.org/10.5194/egusphere-2026-4611
Preprint. Discussion started: 9 November 2026
© Author(s) 2026. CC BY 4.0 License.

using equations (3) to (5), where D is diameter, $\hat{D}$ is the mean diameter, N_0 is number. Geometric standard deviation, σ, for soluble Aitken, accumulation and coarse mode = 1.59, 1.40 and 2.0. The superposition of these modes are shown in blue.

$$\frac{dN}{dlnD} = \frac{N_0}{\sqrt{2\pi}\ln\sigma} e^{\frac{-(\ln D - \ln \bar{D})^2}{2\ln^2\sigma}} \tag{2}$$

$$\frac{dV}{d\ln D} = \frac{V}{\sqrt{2\pi}\ln\sigma} e^{-\frac{(\ln D - \ln Dv)^2}{2\ln^2\sigma}} \tag{3}$$

$$V = N\frac{\pi \bar{D}^3}{6} e^{\frac{9}{2(\ln\sigma)^2}} \tag{4}$$

$$Dv = \bar{D}e^{3\ln^2\sigma} \tag{5}$$

To allow evaluation of SOL/INSOL number and volume distributions throughout the boundary layer, distributions are also shown for model levels 0, 3, 6, 10, 12, equivalent to approximatly 90 (surface), 159, 288, 552 and 724 meters altitude for M293.

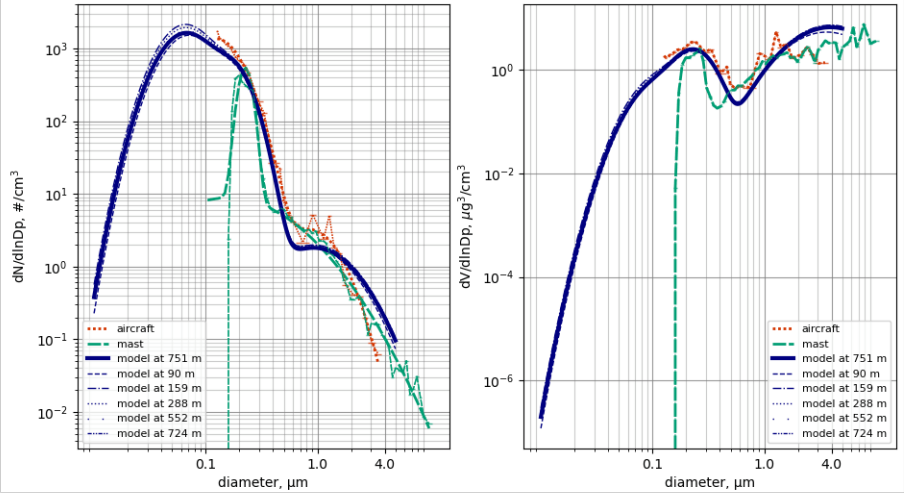

Figure 10. Number (left) and volume (right) PSD for 15th June 2021, from 10:18 to 11:10. Aircraft observed PSD is in red, mast observed PSD in green with SOL/INSOL aircraft-co-located PSD in solid blue. SOL/INSOL predicted PSD at aircraft latitude and longitude at model level 0, 3, 6, 10 and 12 in alternative blue linestyles.

https://doi.org/10.5194/egusphere-2026-4611
Preprint. Discussion started: 9 November 2026
© Author(s) 2026. CC BY 4.0 License.

Figure 10 shows that predicted number and volume distributions are in very good agreement with those observed at the surface and aloft. Modelled PSDs at each altitude are indistinguishable due to the consistent microphysical conditions throughout the well-mixed column. Observed accumulation mode at the surface exhibits a narrower distribution, with the left-hand tail declining at smaller diameters compared with the profiles aloft — likely a result of sampling inconsistencies. The co-located modelled distribution closely replicates the accumulation mode aloft. The model underestimates aerosol concentrations at the smaller end of this size range compared with the airborne measurements, resulting in an underprediction of number concentration in the accumulation mode by modist -25%. The coarse mode is also well captured. The modelled distribution exhibits a lower peak number concentration and a broader spread compared with the observations, resulting in higher number and volume at the larger end of the size range; nevertheless, there is strong agreement overall, with a number concentration difference of only -7% for this mode. Given its importance for ACI and its use in supplying prognostic droplet number concentrations to sub-models such as CASIM, the trends in number concentration described above are also shown in as a timeseries in Appendix E.

Analysis so far provides confidence in CAMSRA initialisation and scaling for realistic $PM_{2.5}$ concentrations and our SOL/INSOL transformations (figure 1) for realistic size distributions.

5.3 Sensitivity testing

To determine the dominant contributions of aerosol chemical species to AOD, $PM_{2.5}$ and size speciation, sensitivity tests (ST) using case M293 are performed by removing sea salt (model suite ST_{SS}), organic matter (ST_{OM}), black carbon (ST_{BC}) and sulphates (ST_{SU}) from the Control simulation's precursor aerosol fields (the CAMSRA initial conditions). The resulting surface level $PM_{2.5}$ (top) and differences in various spatial fields to the control (bottom) are shown in figure 11. PSD for the sensitivity tests are shown in figure 12.

https://doi.org/10.5194/egusphere-2026-4611
Preprint. Discussion started: 9 November 2026
© Author(s) 2026. CC BY 4.0 License.

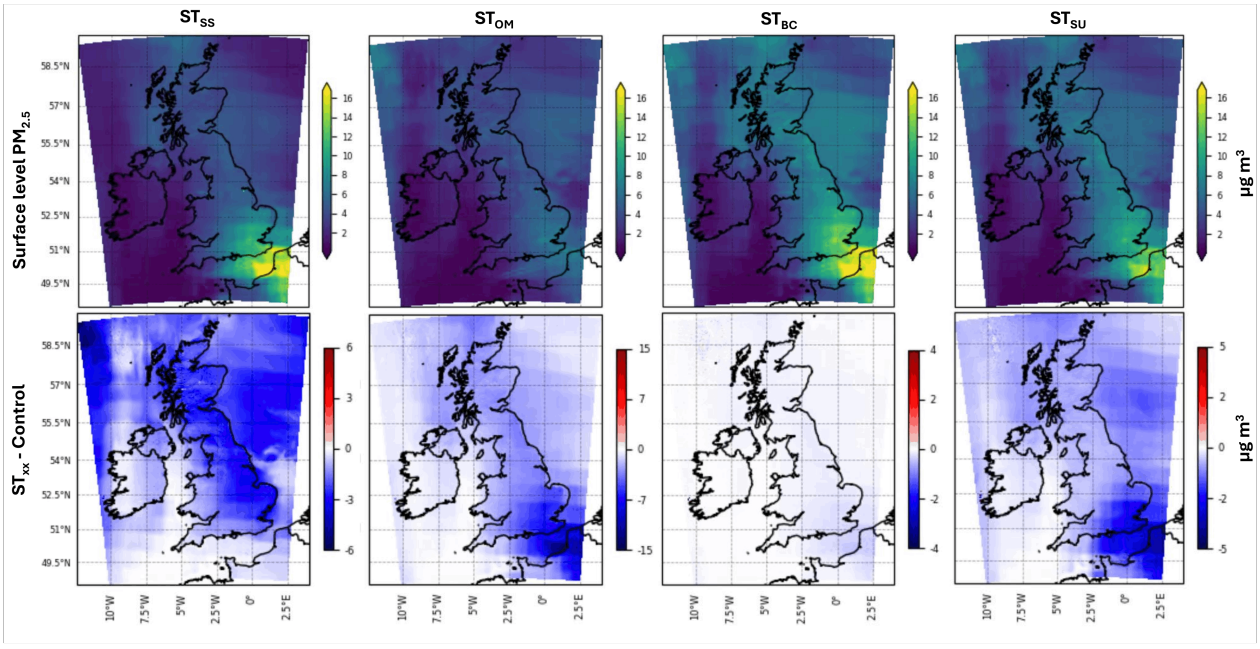

Figure 11. Predicted surface level $PM_{2.5}$ (top, with color scaled to the control simulation for ease of comparison), and predicted minus control simulation surface level $PM_{2.5}$ (bottom) for initial conditions with zero sea salt, zero organic matter, zero black carbon and zero sulphates. All simulations are for case M293 at 13:00 on 15th June 2021.

https://doi.org/10.5194/egusphere-2026-4611
Preprint. Discussion started: 9 November 2026
© Author(s) 2026. CC BY 4.0 License.

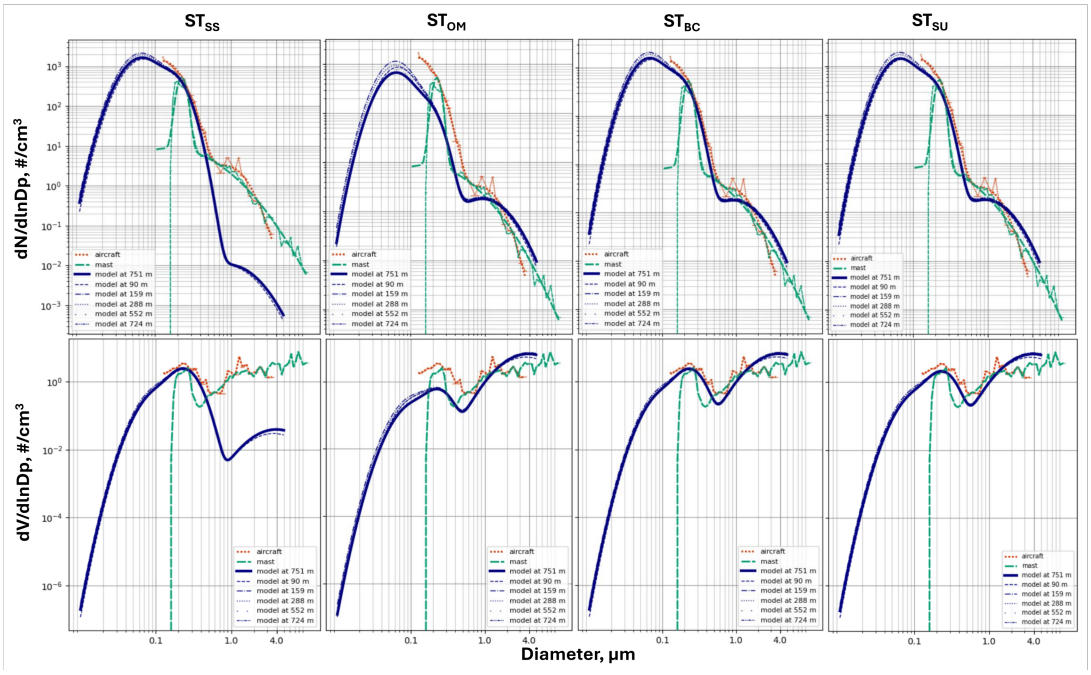

Figure 12. Number size distribtions (top row) and volume size distrbutions (bottom row) for initial conditions with a) zero sea salt b) zero organic matter c) black carbon and d) zero sulphates from 15th June 2021 over aircraft flight times of 14:02 to 14:39. Aircraft PSD is in red (10 second average, straight and level run data), mast PSD in green (10 minute average) with SOL/INSOL-predicted aircraft-co-located PSD in solid blue. SOL/INSOL predicted distributions at aircraft latitude and longitude at model levels 0, 3, 6, 10 and 12 are shown in alternative blue linestyles, with corresponding altitudes in the legend.

As expected, figure 11 shows surface level mass concentration is reduced in all ST configurations when compared to the control suite (figure 5). ST$_{SS}$ shows a reduction of 5 μg m^{-3} which, as shown in fig. 12, impacts the coarse mode only. ST$_{BC}$ shows negligable impact (< 1 μg m^{-3}) on both surface concentration and PSD. ST$_{OM}$ reduces surface PM$_{2.5}$ by approximatly 3 μg m^{-3} and significantly reduces concentrations in the plume in the south east, by 15 μg m^{-3}. This impact is not unexpected given the spatial distribution of the respective CAMSRA constituents discussed in section 5.1 (and shown in appendix D, image D1). The ST$_{OM}$ reduction in PM$_{2.5}$ is pronounced in the accumulation mode as shown in fig 12. The same trends (reduction in surface concentration and plume) are seen in ST$_{SU}$, albeit to a lesser extent (greatest reduction of 5 μg m^{-3} in the plume).

Consistent with the reduction in mass concentration, AOD (not shown) also decreases for each sensitivity test. Removing sea salt aerosol produces the largest reduction of mean AOD (ST$_{SS}$ AOD = 0.09, Control AOD = 0.23). Analysis of soluble coarse mode number concentration for ST$_{SS}$ (not shown), shows that with sea salt removed, substantial coarse mode remains over the ocean, which is due to the primary sea-salt emissions routine occurring before initial aerosol fields are output by the model.

https://doi.org/10.5194/egusphere-2026-4611
Preprint. Discussion started: 9 November 2026
© Author(s) 2026. CC BY 4.0 License.

5.4 Forecast skill test

When operational, given the unavailability of instantaneous CAMSRA initial conditions, SOL/INSOL will be reliant on forecasts (e.g. T+12h). Testing forecast skill is therefore important to evaluate the model's ability to produce accurate and reliable predictions independent of initial-condition variability. Future evaluations will investigate forecast skill up to T+120 hours, over various domains, in preparation for operational use, but here we investigate the short-term predictive forecast skill. We also explore the speciation of aerosol at different lead times to see how fluctuations translate from gridded, speciated ICs to internally-mixed modal distributions.

We again examine case M293, this time initalising the model at 20210615T0000Z, 20210614T1200Z and 20210614T0000Z to give lead times of T+13 (suite Fx_{13}), T+25 (Fx_{25}) and T+37 (Fx_{37}) hours (essentially relying on model forecasting ability to project older CAMSRA aerosol fields forward to the chosen case datetime). These simulations are compared to the control (T+1 hour) and the results are presented in figures 13 and 14 and tables 4 and 5.

The top row of figure 13 (see also figure F1) shows the spatial distribution and mass concentrations of $PM_{2.5}$ at the surface is broadly consistent across the different lead times. Pollutant hotspots (e.g. London) and the ship tracks in the channel remain clearly visible across all lead times, as expected given SOL/INSOL uses monthly average emissions. Notable distinctions between the test simulations and control is the absence of elevated aerosol in the south-east (bottom row, blue areas), and an increase in $PM_{2.5}$ over the south-west quadrant of the domain (bottom row, red areas) in comparison to the control.

https://doi.org/10.5194/egusphere-2026-4611
Preprint. Discussion started: 9 November 2026
© Author(s) 2026. CC BY 4.0 License.

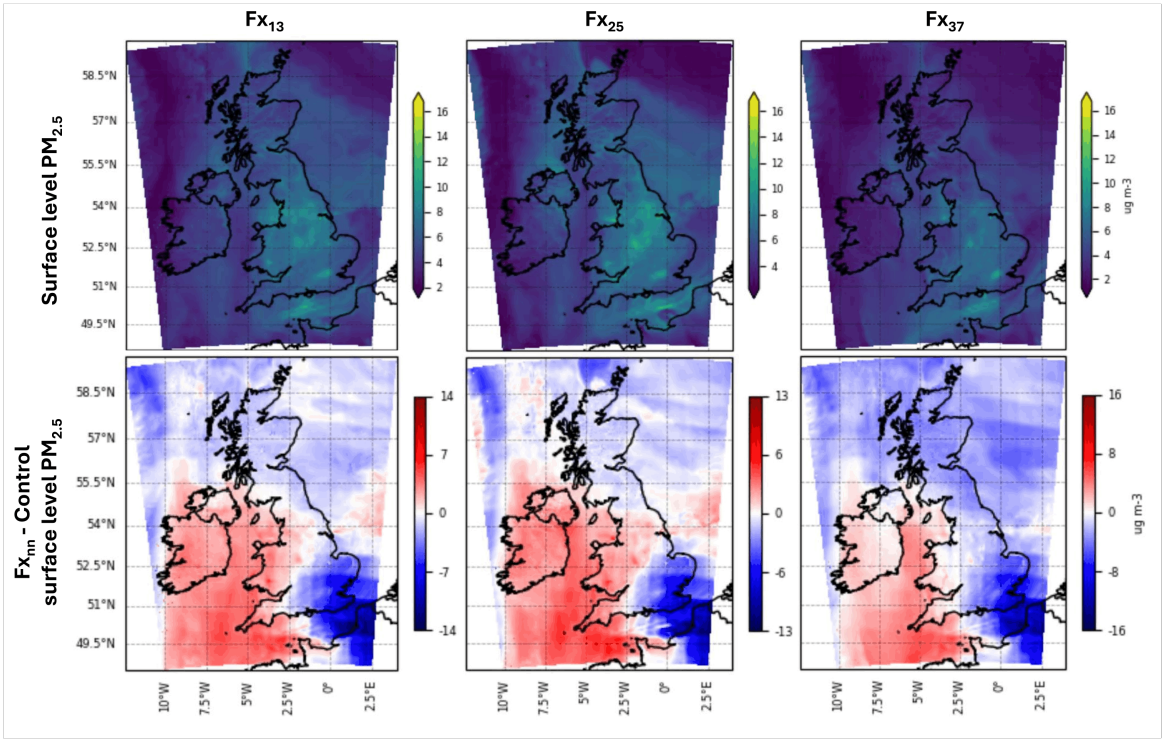

Figure 13. Top: Surface level SOL/INSOL predicted $PM_{2.5}$ over the UKV domain valid for 13:00 on 15th June 2021, initialised at 20210615T0000Z (Fx_{13}), 20210614T1200Z (Fx_{25}) and 20210614T0000Z (Fx_{37}). Color scaled to the Control simulation. Bottom: Difference between the forecast test suites and Control 20210615T1200Z (+1 hrs).

As the forecast lead time grows, the model gradually loses sensitivity to its initial state and becomes increasingly emissions-driven. However, at lead times below 37 hours, initial conditions are expected to remain a dominant factor in determining simulated mass concentrations, particularly in respect of secondary and long-lived species. Therefore, to understand how variations in precursor aerosol speciation from different initialisation dates influence predicted mass concentrations at the forecast date, we analyse the spatial and bulk properties of CAMSRA precursor aerosol across the UKV domain for each initialisation date, and the resulting size distributions.

As expected, the spatial distribution of precurser aerosol for the various initialisation dates (not shown) differ from the control suite due to varying meterology. Individual species are more widely dispersed at longer lead times. Whereas the area of elevated precursor aerosol over the channel is evident at both the surface and in total column burdens in the control suite (T+1 hours), the elevated concentrations are seen at the surface only at longer lead times.

https://doi.org/10.5194/egusphere-2026-4611
Preprint. Discussion started: 9 November 2026
© Author(s) 2026. CC BY 4.0 License.

Considering the area-averaged total column burden of individual precursor species (table 4), notable differences emerge across the different lead times. All precursor aerosol constituents at T+36 hours are significantly lower than the control simulation. T+13 and T+25 hours have more sea salt (significantly +20% at T+25 hours) and more hydrophobic organic matter. In comparison, precursor aerosol at T+1 hour has higher area-averaged sulphates, hydrophillic organic matter and hydrophillic black carbon.

Table 4. Total column burden area averages, in kg kg^{-1}, for black carbon, organic matter, sulphates and sea salt initial conditions for Control, Fx_{13}, Fx_{25} and Fx_{37}

Species	Control	+13 hrs	+25 hrs	+37 hrs
Hydrophobic black carbon	1.65×10^{-07}	1.63×10^{-07}	1.96×10^{-07}	8.51×10^{-08}
Hydrophillic black carbon	7.94×10^{-07}	7.38×10^{-07}	5.56×10^{-07}	4.96×10^{-07}
Hydrophobic organic matter	2.66×10^{-06}	3.06×10^{-06}	3.51×10^{-06}	1.23×10^{-06}
Hydrophillic organic matter	1.73×10^{-05}	1.55×10^{-05}	1.17×10^{-05}	1.06×10^{-05}
Sulphates	5.08×10^{-06}	3.58×10^{-06}	3.13×10^{-06}	3.37×10^{-06}
Sea salt	8.82×10^{-05}	9.30×10^{-05}	1.06×10^{-04}	6.34×10^{-05}

https://doi.org/10.5194/egusphere-2026-4611
Preprint. Discussion started: 9 November 2026
© Author(s) 2026. CC BY 4.0 License.

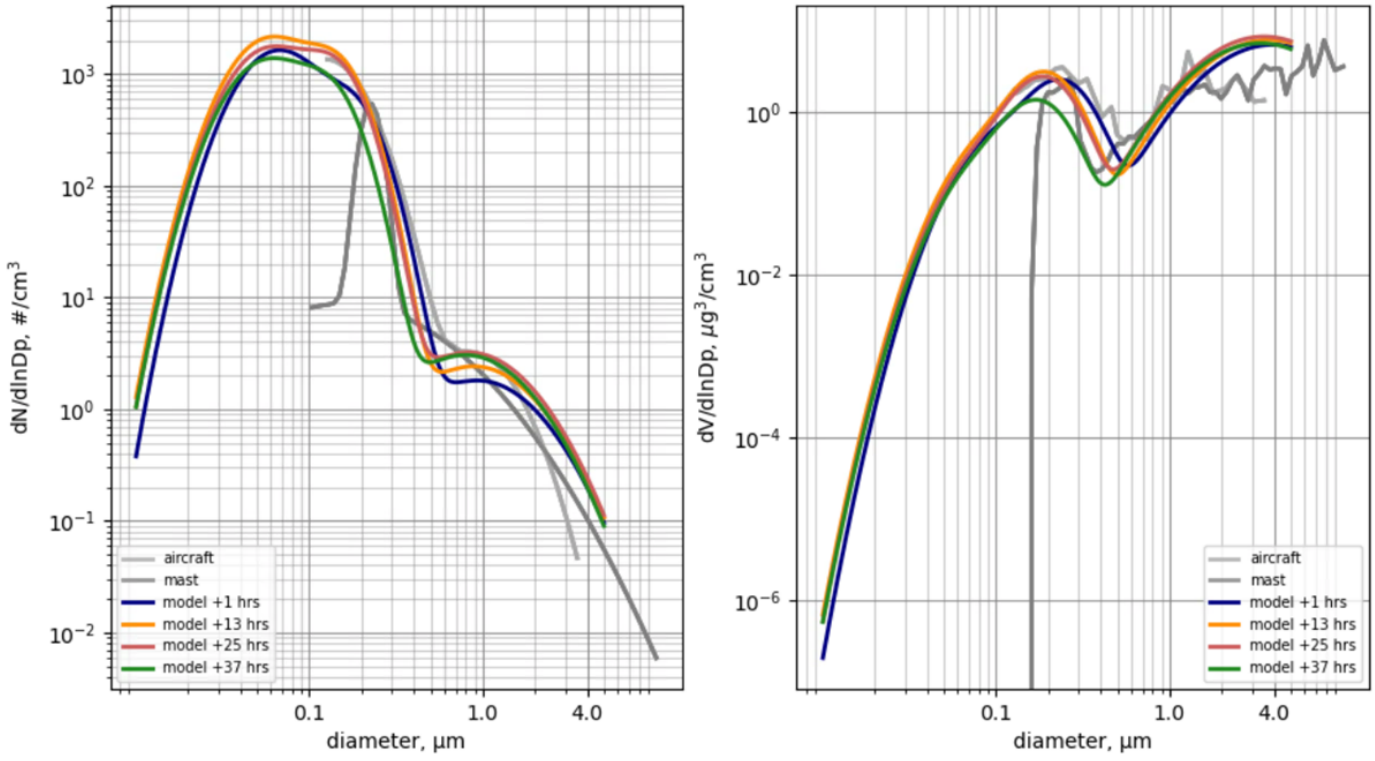

Figure 14. Number (left) and volume (right) particle size distributions for case M293 on 13:00 on 15th June 2021, initialised at 20210615T12000Z (Control, T+1 hr, blue), 20210615T0000Z (Fx_{13}, orange), 20210614T1200Z (Fx_{25} hrs, red) and 20210614T0000Z (Fx_{37}, green)

To understand how fluctuations in precursor aerosol constituents from different initialisation dates translate from gridded, speciated ICs to internally-mixed modal distributions valid on the case date, we again examine PSD. Figure 14 presents the PSDs co-located with the aircraft over the Greater Manchester region at T+1 hour (control, blue), T+13 (orange), T+25 (red) and T+37 (green) hour lead times, alongside the corresponding aircraft and mast observations (grey).

It is immediately evident that the modelled PSDs look very reasonable. The model closely matches the observations across all lead times, although subtle differences are evident. Relative to the control, coarse-mode aerosol is more abundant at all extended lead times. Number concentrations in this mode are within 16.5, 43.19 and 28.08 % (for +13, +25 and +37 hours respectively) of those observed. A modest enhancement in the accumulation mode, compared to the control, is evident at +13 and +25 hour. Here, number concentrations are within 9 and -3 % of those observed. At +37 hours (fig 14, green), there is a marked reduction in comparison to both the control and observations, where number concentrations are -47% of observed.

The forecast test simulations yield UK-wide biases of 4, 12 and -11% for Fx_{13}, Fx_{25} and Fx_{37}, respectively (table 5, appendix F), which fall within the UK median bias of 13% at T+1 hours. In summary, these forecast skill tests suggest that SOL/INSOL retains short-term forecasing skill when initialised from varying aerosol fields, but in consonance with previous findings, enhanced plumes are not captured. This is discussed further in the following chapter.

https://doi.org/10.5194/egusphere-2026-4611
Preprint. Discussion started: 9 November 2026
© Author(s) 2026. CC BY 4.0 License.

Table 5. Mean surface predicted $PM_{2.5}$ with mean observed AURN $PM_{2.5}$ (over 1 hr either side of model time), for 3 case dates. Each simulation has 50 AURN sites.

Case	Date	Mean model over UKV domain ($\pm 2\sigma$)	Mean model over land ($\pm 2\sigma$)	Mean model AURN-CL ($\pm 2\sigma$)	Mean UK-AURN ($\pm 2\sigma$)	NMB (Model AURN-CL VS AURN)
Fx_{13}	20210615T0000Z + 13 hrs	4.93 ± 2.98	5.64 ± 2.89	7.59 ± 3.01	7.32 ± 5.42	0.04
Fx_{25}	20210614T1200Z + 25 hrs	5.27 ± 3.47	6.05 ± 3.25	8.17 ± 3.40	7.32 ± 5.42	0.12
Fx_{37}	20210614T0000Z + 37 hrs	3.77 ± 2.89	4.28 ± 2.82	6.53 ± 3.48	7.32 ± 5.42	-0.11

6 Discussion and conclusions

SOL/INSOL, a new simplified double-moment prognostic aerosol scheme, has been added to UKCA and tested in the Met Office's UKV local area model. A global 20km driving model representative of operational global forecasting system (MOGREPS-G) is used to provide lateral boundary conditions, where initial aerosol conditions are provided by the CAMS Reanalysis dataset. Emissions ancilliaries are monthly means, as used in the Met Office's air quality model. SOL/INSOL uses 4 soluble and 2 insoluble modes with 12 corresponding tracers to provide computationally affordable aerosol representation across NWP timescales. To help evaluate predicted $PM_{2.5}$ mass burdens, microphysics and sensitivity gridded initial conditions converted to modal size distributions, UKV simulations have been compared to a range of surface, mast, airborne and satellite observations. Case study M293 on 15th June 2021, for which airborne data focused on the Manchester region, was selected for indepth analysis, with 30 other cases used to improve the statistical robustness of the evaluation. A number of well-supported results emerge from these simulations.

6.1 M293

M293 shows realistic $PM_{2.5}$ concentrations across the UKV domain and good agreement between predicted co-located and observed surface $PM_{2.5}$. DEFRA (2026) reports mean observed urban-background $PM_{2.5}$ of 7.92 μg m^{-3} for 2021, with which AURN observed $PM_{2.5}$ for the case date is well aligned (7.68μg m^{-3}, noting the AURN mean also includes rural and suburban background sites). Predicted $PM_{2.5}$ over land (6.42μg m^{-3}) is lower than observed - as expected given the land-based domain will be dominated by rural background levels - whereas predicted $PM_{2.5}$ co-located with surface observations is higher (9.14 μg m^{-3}), yeilding a model bias (NMB) of +25% for M293. This indicates SOL/INSOL predicts co-located surface level $PM_{2.5}$ well, albeit with a modest overprediction for this case.

Given the short spin-up time (1 hour) for M293, the dominant influence on the extent and spatial distribution of the predicted aerosol is the initial conditions, rather than meteorology or emissions. Regardless, local hotspots, such as London, which will

https://doi.org/10.5194/egusphere-2026-4611
Preprint. Discussion started: 9 November 2026
© Author(s) 2026. CC BY 4.0 License.

not feature in the coarse-resolution CAMSRA initial conditions, are well represented through higher resolution emissions, even when using monthly mean values.

The agreement between predicted and observed $PM_{2.5}$ indicates that the re-gridded, re-apportioned, and scaled CAMSRA initial conditions perform well. M293 shows an area of enhanced aerosol to the south-east which coincides with spatial features in the CAMSRA constituents (appendix D), in particular black carbon, organic matter and sulphates. The model over-prediction in comparison to observations in this region suggests that CAMSRA may slightly overestimate the long-range transport of aerosol from north-west Europe resulting in the model over predicting in the plume, yeilding a positive model bias for M293.

6.2 Nationwide

Expanding the dataset by 30 case dates strengthens the evidence for good model performance, albeit with a modest model under-prediction of -13% at the surface. DEFRA (2026) show that pollutants (including $PM_{2.5}$ and SO_2) decreased between 2019 and 2022, which corresponds to the period covered by the extended case group (appendix A1). As we adopt 2019 emissions, our prescribed values may be somewhat elevated, implying that the negative model bias could be greater than indicated. The bias varies in sign and magnitude across the individual cases. Differing ICs, orography and meteorological conditions for each case confound attempts to link a single reason for this in the scope of this study. Regardless, figure 6 shows good agreement between modelled and observed surface $PM_{2.5}$ (r = 0.83). The overlap of error bars with the 1:1 line in this figure indicates that this discrepancy between modelled and observed $PM_{2.5}$ cannot be attributed solely to deficiencies in model skill, but may also arise from temporal variability in the observations and spatial variability in the model.

Across the UK, the smallest bias (NMB, surface $PM_{2.5}$) are over summer (2%), and the largest bias over spring and winter (-22%). The small summer bias could be attributed to more accurate emissions scenarios (e.g. more stable domestic heating and transport emissions) or strengthened boundary layer mixing reducing near surface gradients. The larger spring and winter bias may reflect the absence of seasonal nitrate processes in the current configuration, underscoring the potential benefit of implementing the Jones et al. (2021) nitrate scheme in subsequent model iterations. A small bias is also shown for where observed $PM_{2.5}$ is greater than 10 μg m^{-3}. For these enhanced aerosol cases, a combination of small bias (-10%) with low correlation (R^2 = 0.36, figure 6) suggests that while the average aerosol loading is well represented, the model does not capture variability between cases. The low bias for these cases is therefore likely the result of compensating high and low errors rather than accurate simulation of individual events. This is particularly evident in figure A3 for the London region where the majority of enhanced aerosol cases are identified. This result may stem from the use of monthly-mean emissions, which smooth temporal variability, suppress extreme values, and thus limit the model's ability to accuratly reproduce discrete enhanced aerosol events.

Curiously, the median $PM_{2.5}$ across the UKV domain (for 17 of 30 cases) exceeds the land-only value, which is contrary to expectations given the domains exposure to less polluted air masses from the Atlantic ocean (Di Antonio et al., 2023) and the dominance of land-based emissions. This may indicate an issue in either sea-salt initialisation or online generation and is discussed further below.

https://doi.org/10.5194/egusphere-2026-4611
Preprint. Discussion started: 9 November 2026
© Author(s) 2026. CC BY 4.0 License.

6.3 AOD

Although somewhat limited by the availability of satellite coverage, SOL/INSOL is shown to reproduce large scale features seen in AOD retrievals from MODIS: broad country-scale gradients and mesoscale features are represented well. This is supported by a mean R^2 of 0.64 between modelled and observed AOD over 5 cases, suggesting mass and variability - thus total column extinction and spatial patterns of aerosol - are generally well captured by the model, particularly for those cases with higher AOD.

For all 5 cases analysed here, predicted co-located AOD is generally a factor of two lower than observed, which, in consonance with findings above, supports a negative model bias. For case M293, the predicted co-located AOD maximum is markedly lower than observed whereas predicted co-located AOD mean is more aligned, albeit marginally lower. This suggests that, for M293, background AOD is well captured but the model may miss more localised maximas. Prescribing the single scattering albedo (which influences modelled AOD) using low resolution values interpolated onto higher resolutions will lack sub-grid scale aerosol extinction features associated with, e.g., point sources. In future, running the UM at the native grid with a more complex aerosol scheme to generate SOL/INSOL extinction ancillaries at a desired resolution may result in improved representation of the 3D single-scattering albedo and AOD.

6.4 Regional

In contrast to the surface-based UK-wide analysis for M293, which indicates a positive model bias, regional analysis focused on Manchester in north-west England shows a model underprediction (-7%). This region lies well outside the enhanced plume, which is hypothesised to drive the UK-wide overprediction in M293. Augmenting the surface-based observation data with the airborne observations, a well-mixed atmosphere is observed and captured well by the model, with little variation in the vertical. The lower range of airborne observed $PM_{2.5}$ concentrations overlap with the model suggesting the negative bias at the surface likely extends aloft. Model - observation agreement strengthens at the very upper run level ($\sim$ 1100 m), where aircraft observed $PM_{2.5}$ decreases, likely due to being on the perphery of the boundary layer. This brings the model further into alignment at this altitude and suggests a potential difference in modelled boundary layer height. The model profile shows a small reduction (1-2 μg m^{-3}) in aerosol at the lowest model level, likely due to dry deposition of aerosol close to the surface. If this regional effect is consistent across the domain, this near-surface decrease in $PM_{2.5}$ may serve to reduce the surface-based UK-wide positive model bias, in comparison to the rest of the column.

The model employs higher densities (soluble: 1769 kg m^3) than in the observational mass conversion (1640 kg m^3), which - given mass is proportional to density - inflates modelled $PM_{2.5}$. This suggests if densities were aligned, the regional negative model bias would be amplified. It also suggests the regional negative mass bias for M293 can instead be attributed to an underestimate in aerosol volume, likely due to underprediction of particle number or uncertainties in observed particle sizing. To understand this further, number and volume size distributions were examined. Overall, the predicted and observed size and volume distributions show very good agreement for M293. Given that we cannot distinguish between internally and externally mixed aerosol from the observations employed here, this agreement provides confidence that the internal mixing assumed by

https://doi.org/10.5194/egusphere-2026-4611
Preprint. Discussion started: 9 November 2026
© Author(s) 2026. CC BY 4.0 License.

the model is sufficient. Number concentrations are reproduced to within -25% and -7% in the accumulation and coarse modes, respectively, also providing confidence that the initial conditions are well specified. Since the modal distributions are derived from gridded emissions, this agreement is an important validation step. The slightly reduced peak number concentrations in the accumulation and coarse modes for case M293 (Figure 10) support the hypothesis that the regional underprediction in $PM_{2.5}$ is linked to an underestimation of aerosol number. Given the critical role of number concentration in cloud droplet activation within CASIM, this represents another important validation. The magnitude of these differences is modest and suggests sufficiently robust aerosol representation for CASIM applications. Tuning of the scaling factors applied to the CAMSRA accumulation (0.8) and coarse mode (3.0) may improve this agreement further.

For M293, the model demonstrates less horizontal variability than seen in the aircraft observations, and a higher bias aloft (-28%) compared to that at the surface. 71% and 65% of cases in the Manchester and London regions, respectively (table A3 and A4) also show higher bias aloft. This indicates that the model may struggle to reproduce the observed spatial variability, particularly the fine-scale structure sampled by the aircraft. This is common and likley stems from differences in spatial and temporal scaling between the model and observations (Mynard et al., 2023) where natural pollutant variability is observed at scales that are sub-grid to the model, as well as the spatial down-scaling and partitioning of aerosol constituents in the initial conditions. This model is mainly targetting the UK domain, but in the future we may employ the 500 meter London model to see if it improves spatial distribution. In contrast to the Manchester and London regions, 86% of cases over Birmingham (table A2) show higher bias at the surface, indicating surface processes may not be as well captured in this region. Given prognostic models tend to have difficulties simulating accurate meteorological fields in complex topography (Hu et al., 2010), this may be related to the more varied topography in Birmingham region (topographic-map.com, 2026).

sec:st

6.5 Sensitivity tests

Sensitivity tests are conducted to quantify the influence of black carbon, organic matter, sea-salt, and sulphur dioxide from the aerosol precurser fields (CAMSRA) on size distributions and mass concentrations. Removal of organic matter substationally reduces the accumulation mode and the magnitude of the enhanced aerosol seen over the channel, suggesting this species is the main contributor to the plume. As expected, removal of sea-salt has a significant reduction on the coarse mode which produces the largest reduction of mean AOD (ST_{SS} AOD = 0.09, Control AOD = 0.23). This occurs because sea-salt particles are large, highly hygroscopic, and efficient scatterers of light, and because AOD integrates extinction over the entire atmospheric column, thereby capturing substantial maritime aerosol burdens. Consequently, sea-salt aerosol exerts a disproportionately strong influence on column-integrated extinction despite contributing little to surface $PM_{2.5}$. Notably, with sea salt removed, a substantial coarse mode remains over the ocean. This is due to sea salt generated online in UKCA, which may be responsible for the higher $PM_{2.5}$ concentrations over the UKV domain compared to land only, as discussed above. Given the influence that modal sea-salt distributions exert on aerosol optical properties in these tests, the enhanced online generation scheme may substantially affect the derivation of AOD and warrants further investigation.

https://doi.org/10.5194/egusphere-2026-4611
Preprint. Discussion started: 9 November 2026
© Author(s) 2026. CC BY 4.0 License.

6.6 Forecast skill

When operational, SOL/INSOL will be initialised by forecasts and therefore the ability to produce accurate and reliable predictions independent of initial-condition variability is important. To evaluate SOL/INSOL's short term predictive forecast skill case M293 was initialised at T+13, T+25 and T+37 hours.

Results show two notable distinctions between the forecast test suites and the control; firstly, an increase in $PM_{2.5}$ in the south-west (figure 13, red area) and secondly the absence of enhanced aerosol in the south-east (blue). The latter anomaly is consistent with the other evaluations presented here; reinforcing that the model struggles to accurately reproduce enhanced aerosol events.

Analysis of aerosol precursor speciation at different initialisation times, and their transformation from gridded fields into internally mixed modal size distributions at forecast time, provides insight into differences in the particle size distribution (PSD). Variability in individual precursor components aids in identifying the drivers of these anomalies.

Regional number and volume distributions (fig 14) closely match observations across all lead times. Relative to both the control and observations, there is more coarse-mode aerosol at every lead time. For +13 and +25 hours, this is driven by an increase in sea-salt ICs (table 4). At T+37 hours (fig 14, green), sea-salt ICs decrease, indicating that the coarse-mode increase at this lead time must be regional or generated online. Regardless, at T +37 hours, a marked reduction (-47%) in regional accumulation mode number concentration coincides with the reduction of all precursor aerosol constituents for this simulation - effectively counteracting any regional enhancement in the coarse mode to yield an overall UK-wide negative model bias of -11%.

In comparison to the control suite, an enhancement in regional accumulation mode is evident at +13 and +25 hour lead times, which brings these into closer alignment with observations. This behaviour coincides with an increase in hydrophobic organic matter and sea salt for these initialisation times, indicative of primary aerosol. Latitudinal cross sections of the domain (not shown) indicate that this increase in accumulation-mode precursor aerosol is the primary driver of the area of enhanced mass in the south-west at longer leadtimes. This increase in accumulation mode corresponds to a UK-wide positive model bias of 4% and 12% for T+13 and T+25 hours (table 5).

The area of enhanced aerosol in the south-east is evident in the precursor aerosol at the surface only at T+13 and T+25 hours, whereas it is evident both at the surface and in total column burdens at T+1 hour. The precursor aerosol at +1 hour has higher area-averaged sulphates, hydrophillic organic matter and hydrophillic black carbon indicative of aged continential aerosol (Mann et al., 2010). Dunkerque industrial emissions - the likely point source for this area of enhanced aerosol for M293 - are scaled by 0.1 in alignment to the operational air quality model (section 2.2). Therefore, at longer lead times, the enhanced primary aerosol initialised near the surface may be removed through deposition processes and not sufficiently replenished by ongoing emissions from this point source. This basic analysis of aerosol composition suggests this may account for the absence of the enhanced aerosol signature over the south-east at longer lead times, however, given the lack of nitrates in the CAMSRA initial conditions, it cannot be conclusively said that it is not semi-volatile organic species such as nitrate. This shortfall in model fidelity is being reviewed in depth but is outside the scope of this evaluation.

https://doi.org/10.5194/egusphere-2026-4611
Preprint. Discussion started: 9 November 2026
© Author(s) 2026. CC BY 4.0 License.

For M293, regional perturbations in modal size distributions appear broadly consistent with the UK-wide surface bias, suggesting that the processes governing these shifts are not unique to the Manchester region but reflect systematic, national-scale model tendencies. This is not unexpected, given that the CAMS precursor aerosols have been regridded from a coarser spatial resolution. These transitions illustrate how variations in the relative contributions of initial aerosol components translate into systematic changes in particle size distributions and associated mass concentrations, most notably at T+37 hours where reductions across all precursor aerosol constituents translates to lower accumulation-mode aerosol at the forecast date, which leads to an overall negative domain-wide bias.

An increase in model bias as lead time increases is expected, given a known shortcoming of prognostic models is prediction errors due to imperfections in the initial conditions (Hu et al., 2010). Here, model bias is very low at T+13 hours (4%, significant to future operational initialisation lead times) and increases to 12 and -11 % at T+25 and T+37 hours. Regardless, these biases fall comfortably in line with the median bias across all extended case studies at T+1 hours (-13%, table 3), demonstrating that SOL/INSOL retains useful short-term forecast skill when initialised from varying aerosol fields, with broadly consistent spatial $PM_{2.5}$ patterns across lead times up to T+37 hours. This analysis further supports an ICs-driven model at these short lead times and highlights the importance of aerosol initialisation species apportionment and emissions representation to ensure fidelity of $PM_{2.5}$ mass concentrations.

6.7 Concluding remarks

In conclusion, this first evaluation of SOL/INSOL demonstrates excellent fidelity with observations, delivering skilful and computationally efficient aerosol representation across NWP timescales.

CAMS reanalysis initial conditions perform very well. While emissions increasingly dominate the simulations as lead time increases, initial-condition differences remain influential at the shorter lead times evaluated here, particularly through changes in aerosol speciation and modal partitioning. Variations in the relative contributions of aerosol components, in particular sea-salt which is seen to have a significant impact on AOD, translate into systematic changes in particle size distributions and associated mass concentrations.

Number concentrations generally agree well with those observed across the accumulation and coarse modes, paticularily at lead times of less than +37 hours. This development enables consistent coupling of droplet number concentration within CASIM which will strengthen the model's treatment of aerosol–cloud interactions. SOL/INSOL is shown to maintain short-term forecast skill with broadly consistent spatial $PM_{2.5}$ patterns across lead times up to 37 hours, representing background aerosol loadings with fidelity.

SOL/INSOL is currently limited in its ability to accurately reproduce discrete enhanced aerosol events and emissions require tuning to address this shortfall; in particular a review of point source emissions scaling. In future we will look to run a more comprehensive evaluation into emissions accuracy and its impact on forecasting skill, implement the Jones et al. (2021) nitrate scheme (including full chemistry with + nitrates and ammonium), and compare CAMSRA to the +12 hour CAMS Forecast as global percursor aerosol in a step towards operational implementation. A postliminary review is currently underway examining the 2-way coupling of SOL/INSOL with CASIM and its implications for ACI and hydrology.

https://doi.org/10.5194/egusphere-2026-4611
Preprint. Discussion started: 9 November 2026
© Author(s) 2026. CC BY 4.0 License.

Code availability. The UM and CASIM code branches used in the publication have not all been submitted for review and inclusion in the UM/CASIM trunk or released for general use. The UKCA code used in the publication has been committed to the UKCA code trunk, having passed both science and code reviews according to the working practices. Please note, at the time of the work for this paper they were branches to UM-UKCA version stated in the paper. The JULES code used in the publication has been committed to the JULES code trunk, having passed both science and code reviews according to the JULES working practices; in the JULES version stated in the paper.

Data availability. The UM output used to produce figures 5-14, tables 3, 5 as well as supplementary figures A1-A3, E1-G1 and supplementary tables A1-A4 is available from the Centre of Environmental Data Analysis (CEDA) via doi:10.5285/2de684c1211e4d89a5deba150eeb3689. CAMS Reanalysis data is from https://ads.atmosphere.copernicus.eu/datasets/cams-global-reanalysis-eac4?tab=overview (last access: 2nd July 2026). Emissions data is from the following sources: NAEI: https://naei.energysecurity.gov.uk/ (last access: 2nd July 2026), MEGAN-MACC as per Sindelarova et al. (2014) from https://eccad.aeris-data.fr/ (last access: 2nd July 2026), EMEP from https://www.emep.int/ (last access: 2nd July 2026). OSCA mast site data is available on CEDA: http://catalogue.ceda.ac.uk/uuid/65b50d3348cb4745bb7acfcf6f2057b8, Watson et al. (2023). AURN surface observation data is from DEFRA: https://uk-air.defra.gov.uk/networks/network-info?view=aurn. MOASA Clean Air project data is available from CEDA via DOI:10.5285/0AA1EC0CF18E4065BDAE8AE39260FE7D, Mynard et al. (2023). Finally, MODIS data is aquired via NASA Earthdata: https://search.earthdata.nasa.gov/search?fst0=atmosphere

https://doi.org/10.5194/egusphere-2026-4611
Preprint. Discussion started: 9 November 2026
© Author(s) 2026. CC BY 4.0 License.

Appendix A: National and regional case summaries

A1 UK-WIDE CASES

Table A1. Predicted and observed surface $PM_{2.5}$ for 31 case dates across the UK. For each case, the table shows surface SOL/INSOL predicted $PM_{2.5}$ across the UKV domain, over the UK land only and co-located (CL) with UK-wide AURN sites, alongside mean observed UK-wide AURN $PM_{2.5}$ (over 1 hour either side of model time of 13:00). The final column shows the mean NMB for model AURN-CL against AURN $PM_{2.5}$. "No. AURN sites" is the number of AURN observation sites available for each case date. The final 7 rows show grand medians (the median over 31 case study means) categorised as follows: over all cases ("MEDIAN"), those cases when AURN observed $PM_{2.5}$ >= 10 μg m^{-3} ("AURN OVER 10"), when AURN observed $PM_{2.5}$ < 10 μg m^{-3} ("UNDER AURN 10"), and for seasonal splits (where "SUMMER" = JJA, "AUTUMN" = SON, "WINTER" = DJF and "SPRING" = MAM). The numbers in brackets in the row header indicates how many cases were used to calculate each respective median (noting the AUTUMN median is absent due to just one case falling in this category). Cases highlighted in bold are those which had sufficient satellite coverage to enable meaningful comparison of AOD.

Case	Date	No. AURN sites	Mean model over UKV domain	Mean model over land	Mean model AURN-CL	Mean UK-AURN	NMB
M290	20210609	50	3.74	2.83	2.87	4.32	-0.34
M291	20210610	50	3.11	2.19	2.98	3.23	-0.08
M295	20210623	49	4.75	5.22	8.64	8.46	0.02
M310	20220127	47	3.09	2.04	3.29	5.23	-0.37
M312	20220202	45	2.35	1.98	3.56	4.49	-0.21
M313	20220203	46	2.46	1.99	2.28	3.46	-0.34
M316	20220210	47	5.99	5.73	5.99	5.52	0.08
M292	20210614	50	6.26	5.37	5.99	5.88	0.02
M293	20210615	50	5.19	6.42	9.14	7.32	0.25
M298	20210708	49	3.43	3.87	5.79	6.03	-0.04
M299	20210709	50	4.44	5.87	8.94	6.65	0.34
M300	20210720	47	11.95	12.85	18.01	9.73	0.85
M317	20220211	47	2.78	2.77	4.72	8.02	-0.41
M320	20220301	47	4.50	4.90	6.44	7.43	-0.13
M275	20201126	50	2.26	2.85	7.17	11.70	-0.39
M276	20201201	49	3.07	2.58	5.64	5.91	-0.05
M277	20201209	50	2.54	2.86	6.31	7.70	-0.18
M278	20201217	49	2.31	1.60	3.57	5.66	-0.37
M279	20210308	48	8.17	9.02	12.29	16.97	-0.28
M282	20210319	49	2.55	2.93	3.83	2.95	0.30
M287	20210422	50	9.68	5.97	4.57	8.12	-0.44
M294	20210616	50	5.61	4.95	4.26	5.77	-0.26
M297	20210702	50	7.46	9.29	13.19	13.76	-0.04
M302	20210722	46	15.83	18.15	22.35	11.89	0.88
M311	20220128	48	3.70	3.76	7.05	9.21	-0.24
M314	20220204	47	3.98	2.79	3.64	3.92	-0.07
M315	20220208	46	3.04	1.99	1.84	3.46	-0.47
M319	20220225	48	5.28	4.45	6.35	6.64	-0.04
M323	20220310	48	6.58	5.20	5.97	8.02	-0.26
M324	20220314	47	3.67	3.13	3.67	4.70	-0.22
M325	20220324	49	17.90	16.09	24.90	27.56	-0.10
MEDIAN (31)			3.98	3.87	5.97	6.64	-0.13
AURN OVER 10 (5)			8.17	9.29	13.19	13.76	-0.10
AURN UNDER 10 (26)			3.72	3.45	5.18	5.90	-0.16
SUMMER (11)			5.19	5.37	8.64	6.65	0.02
AUTUMN (1)			-	-	-	-	-
WINTER (12)			3.06	2.67	4.18	5.59	-0.22
SPRING (7)			6.58	5.20	5.97	8.02	-0.22

https://doi.org/10.5194/egusphere-2026-4611
Preprint. Discussion started: 9 November 2026
© Author(s) 2026. CC BY 4.0 License.

A2 REGIONAL CASE SUMMARY TABLES

Tables A2, A3 and A4. Birmingham, Manchester and London based case studies showing mean aircraft (AC) co-located (CL) SOL/INSOL predicted $PM_{2.5}$ alongside mean AC $PM_{2.5}$, and AURN-CL model $PM_{2.5}$ alongside the mean $PM_{2.5}$ from AURN sites within 12 km of the AC transect, averaged over the aircraft transect times, "AC times". Nominal Mean Bias (NMB) is derived for AC-Cl model against AC $PM_{2.5}$, and AURN-CL model against AURN site $PM_{2.5}$. "AC datapoints" gives the number of values used to derive the AC-CL model mean, AC mean and associated NMB. "AURN datapoints" gives the number of values used to derive AURN-CL model mean, AURN mean and associated NMB. Grand means (final 7 rows) categorise the cases as follows: all cases ("MEAN"), those cases when AURN observed $PM_{2.5}$ >= 10 μg m^{-3} ("AURN OVER 10"), when AURN observed $PM_{2.5}$ < 10 μg m^{-3} ("MEAN UNDER AURN 10"), and for seasonal splits (where "SUMMER MEAN" = JJA, "AUTUMN MEAN" = SON, "WINTER MEAN" = DJF and "SPRING MEAN" = MAM). The numbers in brackets in the final 7 row headers indicate how many cases were used to calculate each respective mean. Those cases highlighted in bold are the five which had sufficient satellite coverage to enable meaningful comparison of AOD.

Table A2. Birmingham

Case	AC mean altitude (m)	AC times	AC datapoints	AURN datapoints	AC-CL model mean	AC mean	NMB	AURN-CL model mean	AURN mean	NMB
M290	431-1130	2021-06-09 11:58 to 13:00	374	5	2.93	4.34	-0.32	2.96	4.61	-0.36
M291	414-1281	2021-06-10 11:43 to 12:50	400	5	2.90	2.94	-0.01	3.26	2.18	0.49
M295	424-682	2021-06-23 11:39 to 13:21	615	5	11.53	10.83	0.07	11.57	12.70	-0.09
M310	382-670	2022-01-27 13:46 to 14:58	431	3	1.47	1.66	-0.12	2.37	4.79	-0.50
M312	401-691	2022-02-02 12:43 to 14:08	512	4	2.11	2.07	0.02	3.66	2.48	0.47
M313	392-696	2022-02-03 13:02 to 14:23	486	4	1.24	2.12	-0.42	1.95	2.45	-0.21
M316	380-1243	2022-02-10 12:25 to 14:14	658	4	4.94	3.37	0.47	5.70	4.53 2	0.26
MEDIAN (7)					2.90	2.94	-0.01	3.26	4.53	-0.09
MEDIAN OVER AURN 10 (1)					-	-	-	-	-	-
MEDIAN UNDER AURN 10 (6)					2.51	2.53	-0.06	3.11	3.51	0.03
SUMMER MEDIAN (3)					2.93	4.34	-0.01	3.26	4.61	-0.09
AUTUMN MEDIAN (0)					-	-	-	-	-	-
WINTER MEDIAN (4)					1.79	2.09	-0.05	3.02	3.51	0.03
SPRING MEDIAN (0)					-	-	-	-	-	-

https://doi.org/10.5194/egusphere-2026-4611
Preprint. Discussion started: 9 November 2026
© Author(s) 2026. CC BY 4.0 License.

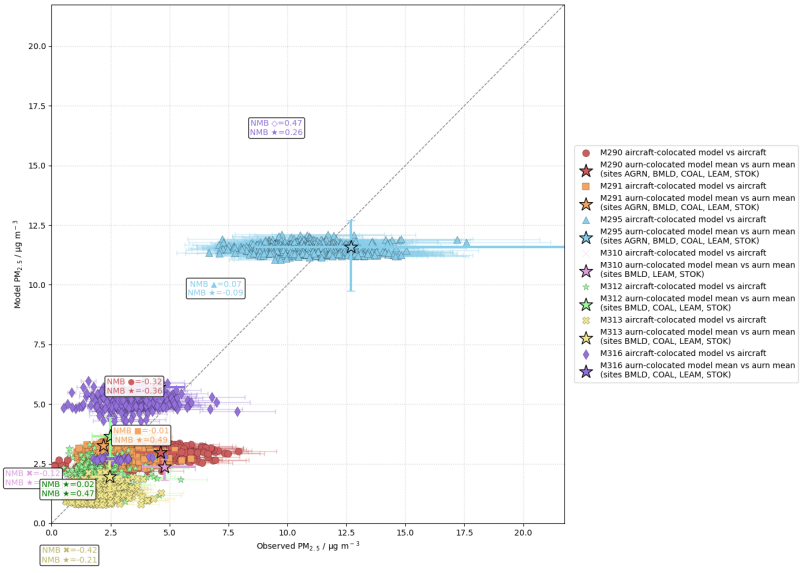

Figure A1. Brum dv141.

Table A3. Manchester

Case	AC mean altitude (m)	AC times	AC data-points	AURN data-points	AC-CL model mean	AC mean	NMB 1	AURN-CL model mean	AURN mean	NMB 2
M292	350-1099	2021-06-14 14:54 to 15:55	365	6	5.89	4.74	0.24	6.03	5.10	0.18
M293	358-1094	2021-06-15 10:18 to 11:09	310	6	6.64	9.21	-0.28	7.08	7.63	-0.07
M298	409-1009	2021-07-08 14:05 to 15:52	648	6	4.83	5.11	-0.05	5.03	4.42	0.14
M299	658-972	2021-07-09 10:33 to 11:22	296	6	5.01	7.58	-0.34	5.57	6.74	-0.17
M300	694-999	2021-07-20 14:02 to 14:39	224	6	10.39	6.40	0.62	9.91	5.12	0.94
M317	383-795	2022-02-11 12:12 to 13:43	550	6	2.53	4.98	-0.49	4.56	7.89	-0.42
M320	403-941	2022-03-01 13:26 to 13:51	156	6	7.47	4.41	0.69	7.33	5.88	0.25
MEDIAN (7)					5.89	5.11	-0.05	6.03	5.88	0.14
MEDIAN OVER AURN 10 (0)					-	-	-	-	-	-
MEDIAN UNDER AURN 10 (7)					5.89	5.11	-0.05	6.03	5.88	0.14
SUMMER MEDIAN (5)					5.89	6.40	-0.05	6.03	5.12	0.14
AUTUMN MEDIAN (0)					-	-	-	-	-	-
WINTER MEDIAN (1)					-	-	-	-	-	-
SPRING MEDIAN (1)					-	-	-	-	-	-

https://doi.org/10.5194/egusphere-2026-4611
Preprint. Discussion started: 9 November 2026
© Author(s) 2026. CC BY 4.0 License.

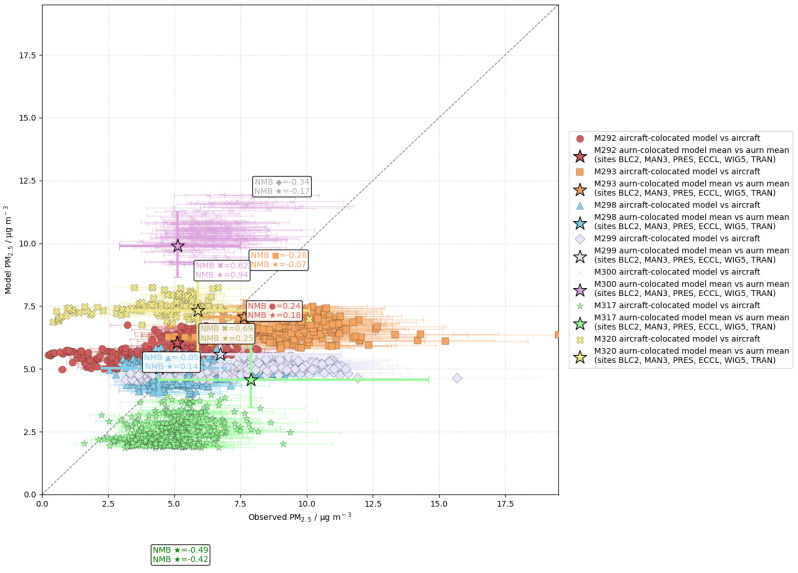

Figure A2. Manc.

Table A4. London

Case	AC mean altitude (m)	AC times	AC data-points	AURN data-points	AC-CL model mean	AC mean	NMB	AURN-CL model mean	AURN mean	NMB
M275	170-518	2020-11-26 12:25 to 13:41	457	7	3.01	5.43	-0.45	11.91	14.72	-0.19
M276	155-536	2020-12-01 12:12 to 13:24	437	7	4.62	6.09	-0.24	6.90	6.26	0.10
M277	161-535	2020-12-09 11:56 to 13:33	586	7	3.20	8.18	-0.61	6.97	7.66	-0.09
M278	272-519	2020-12-17 12:11 to 13:28	463	7	2.09	8.04	-0.74	6.42	6.10	0.05
M279	164-536	2021-03-08 14:20 to 15:57	587	7	13.78	24.01	-0.43	18.90	26.97	-0.30
M282	176-523	2021-03-19 12:30 to 13:45	451	7	4.98	5.68	-0.12	6.05	4.67	0.29
M287	168-521	2021-04-22 11:25 to 12:22	341	7	5.02	7.18	-0.30	5.35	10.17	-0.47
M294	414-678	2021-06-16 11:11 to 12:38	523	6	4.95	6.97	-0.29	4.97	6.80	-0.27
M297	153-659	2021-07-02 11:15 to 12:48	557	6	17.42	17.49	-0.00	16.11	15.42	0.04
M302	177-545	2021-07-22 11:04 to 12:11	400	6	21.40	10.65	1.01	21.18	9.86	1.15
M311	385-501	2022-01-28 12:45 to 13:40	333	6	3.17	6.90	-0.54	15.15	10.09	0.50
M314	158-464	2022-02-04 12:34 to 13:37	380	6	2.96	1.28	1.31	4.43	3.00	0.48
M315	158-555	2022-02-08 11:51 to 13:39	645	6	0.57	1.98	-0.71	2.02	2.54	-0.21
M319	153-468	2022-02-25 12:14 to 13:49	571	6	5.30	5.91	-0.10	6.08	6.06	0.00
M323	168-661	2022-03-10 12:10 to 13:50	599	6	7.63	9.10	-0.16	8.31	10.62	-0.22
M324	180-593	2022-03-14 12:05 to 13:19	445	5	1.68	4.27	-0.61	2.77	5.76	-0.52
M325	341-608	2022-03-24 12:16 to 13:39	500	6	20.93	18.90	0.11	31.01	24.48	0.27
MEDIAN (17)					4.95	6.97	-0.29	6.90	7.66	0.00
MEDIAN OVER AURN 10 (7)					7.63	9.10	-0.30	15.15	14.72	-0.19
MEDIAN UNDER AURN 10 (10)					3.91	6.00	-0.26	6.07	6.08	0.03
SUMMER MEDIAN (3)					17.42	10.65	-0.00	16.11	9.86	0.04
AUTUMN MEDIAN (1)					-	-	-	-	-	-
WINTER MEDIAN (7)					3.17	6.09	-0.54	6.42	6.10	0.05
SPRING MEDIAN (6)					6.33	8.14	-0.23	7.18	10.39	-0.26

https://doi.org/10.5194/egusphere-2026-4611
Preprint. Discussion started: 9 November 2026
© Author(s) 2026. CC BY 4.0 License.

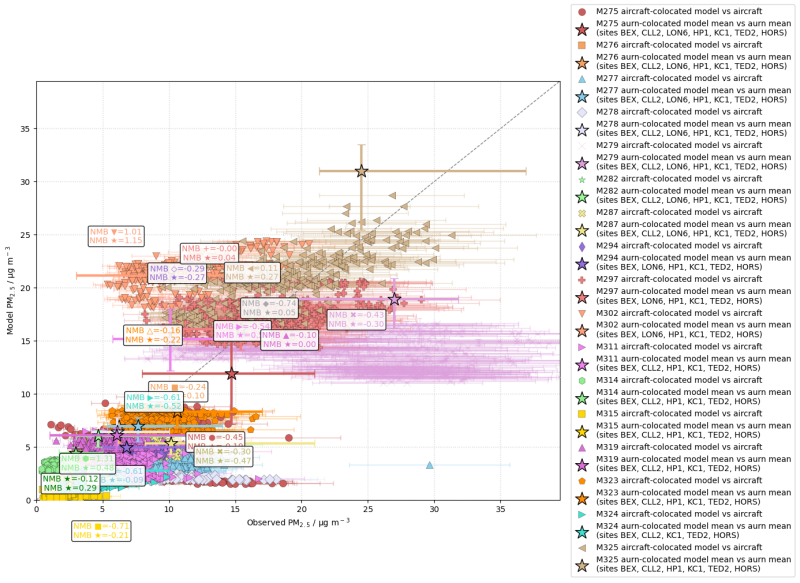

Figure A3. London (dv137)

Appendix B: SEVIRI dust RGB

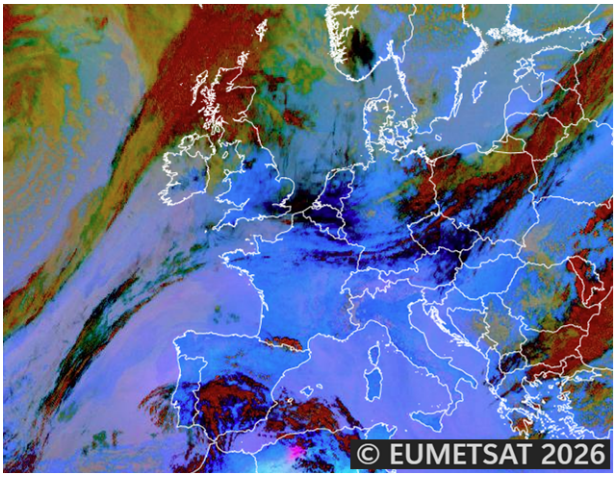

Figure B1. SEVIRI dust RGB (Red, Green, Blue) composite for 12:00 UTC on 15th June 2021. Based upon infrared channel data from the Meteosat Second Generation satellite. The color of dust varies from pink to violet. EUMETSAT Meteosat data 2026.

https://doi.org/10.5194/egusphere-2026-4611
Preprint. Discussion started: 9 November 2026
© Author(s) 2026. CC BY 4.0 License.

Appendix C: EasyAerosol derived short-wave single scattering albedo

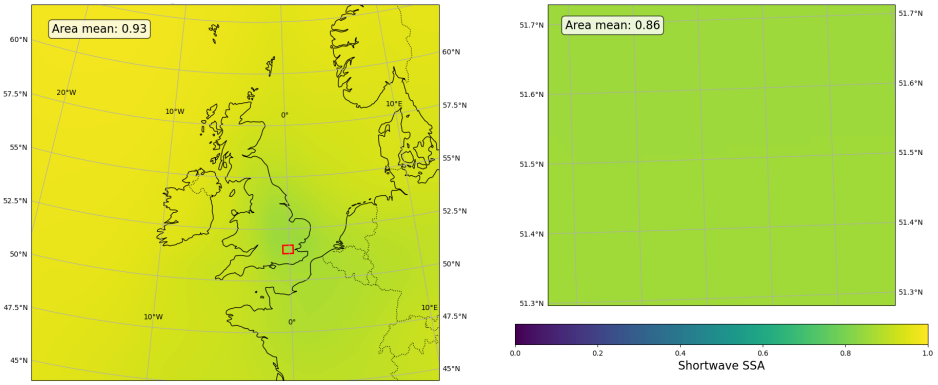

Figure C1. EasyAerosol derived short-wave single scattering albedo for the 505 - 690 nm waveband, for July, at 955 m level height over the UK, as prescribed for SOL/INSOL. Greater London area, red rectangle, has an average SSA of 0.86.

https://doi.org/10.5194/egusphere-2026-4611
Preprint. Discussion started: 9 November 2026
© Author(s) 2026. CC BY 4.0 License.

Appendix D: CAMS Reanalysis precursor aerosol

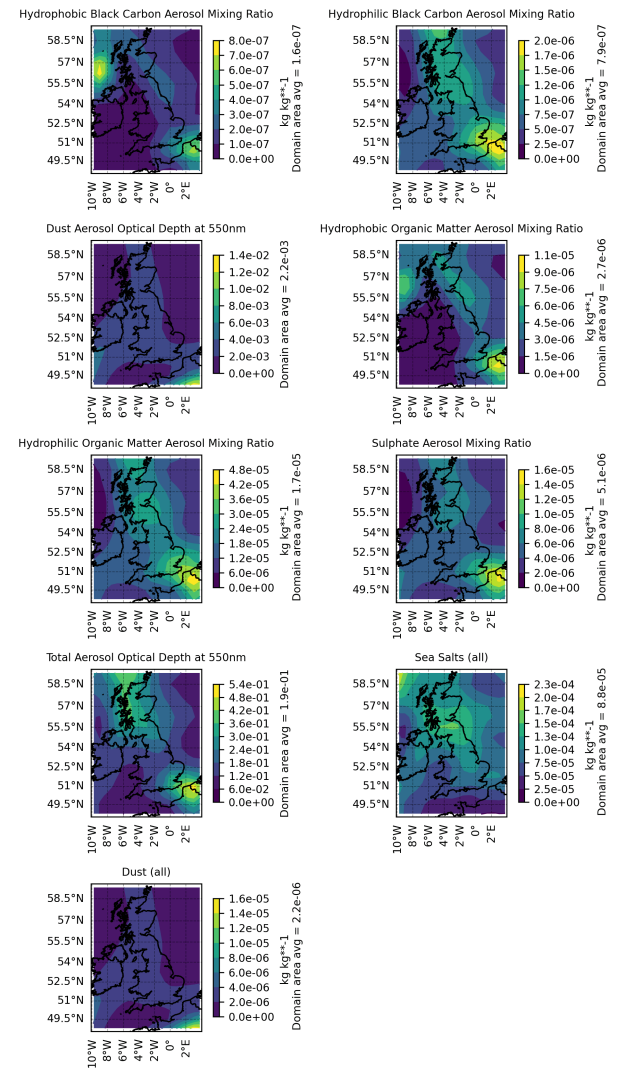

Figure D1. CAMS Reanalaysis aerosol optical depth and aerosol constituents total column burdens for 13:00 UTC 15th June 2021, regridded to UKV resolution. The domain area average is shown alongside the colorbar.

https://doi.org/10.5194/egusphere-2026-4611
Preprint. Discussion started: 9 November 2026
© Author(s) 2026. CC BY 4.0 License.

Appendix E: Number concentration

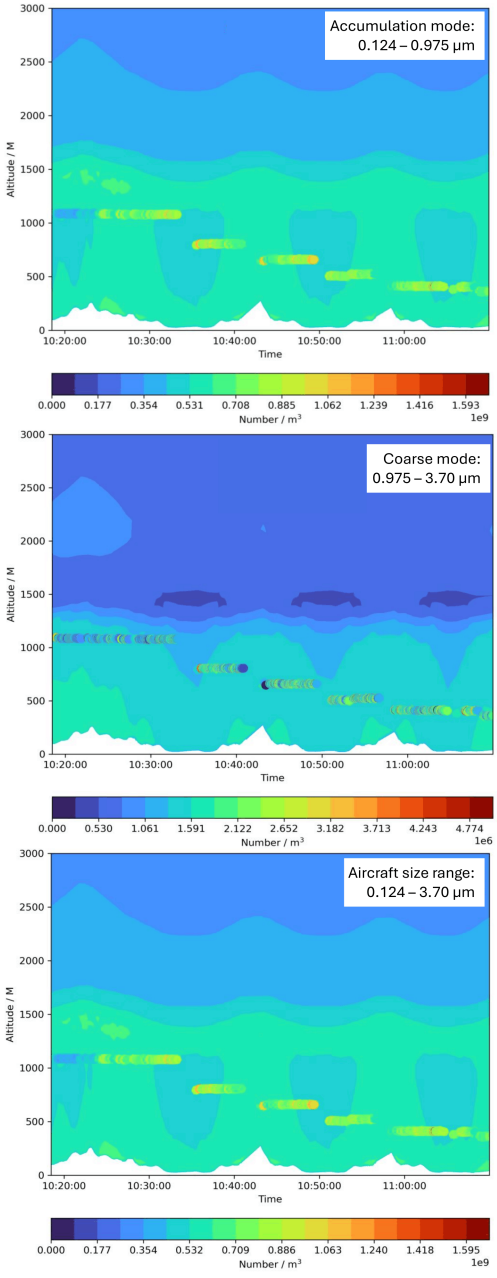

Figure E1. Foreground: Aircraft number concentration for case M293 on 15th June 2021 from 10:18 to 11:09 for the accumulation mode (top, 0.124 - 0.975 μm), coarse mode (middle, 0.975 - 3.70 μm) and the aircraft size range (bottom, 0.124 - 3.70 μm). Background: control simulation number concentration co-located with aircraft latitude and longitude from 13:00 on 15th June 2021, integrated over the corresponding size ranges. The under-prediction of modelled number concentration in comparison to the aircraft corresponds to -25% in the accumulation mode and -7% in the coarse mode, as discussed in section 5.2.1

https://doi.org/10.5194/egusphere-2026-4611
Preprint. Discussion started: 9 November 2026
© Author(s) 2026. CC BY 4.0 License.

Appendix F: Forecast skill $PM_{2.5}$ maps

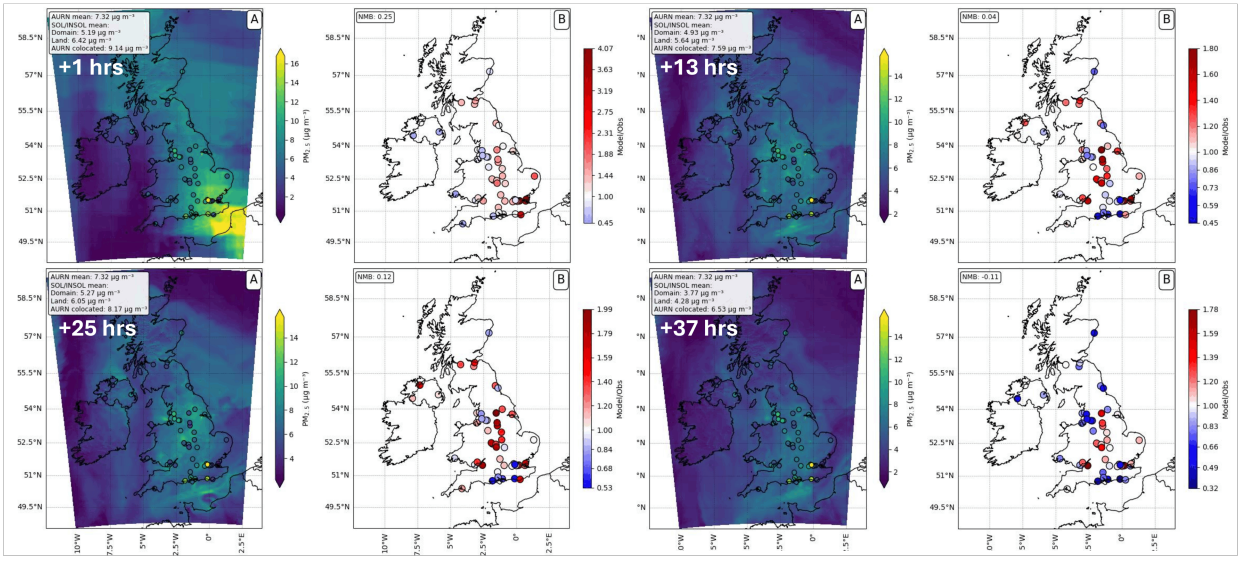

Figure F1. UK-wide surface level SOL/INSOL and AURN $PM_{2.5}$ for case M293, initalised at 20210615T12000Z, 20210615T0000Z, 20210614T1200Z and 20210614T0000Z to give lead times of T+1 (control), T+13 (suite Fx_{13}), T+25 (Fx_{25}) and T+37 (Fx_{37}) hours. For each simulation, panel A shows surface level SOL/INSOL predicted $PM_{2.5}$ over the UK for 13:00 on 15th June 2021, overlaid with mean urban background AURN $PM_{2.5}$ (circles) from 12:00 - 14:00. The colorscale range spans the 1st to 99th percentiles of the data from both datasets. The legend provides mean UK-wide AURN alongside mean SOL/INSOL over the UKV domain, over land only and co-located with the AURN sites. Panel B: SOL/INSOL co-located $PM_{2.5}$ divided by AURN $PM_{2.5}$ mean, where a score of 1 (white) indicates agreement between datasets, >1 (red) indicates model over-prediction and <1 (blue) indicates model underprediction.

https://doi.org/10.5194/egusphere-2026-4611
Preprint. Discussion started: 9 November 2026
© Author(s) 2026. CC BY 4.0 License.

Appendix G: AOD, additional cases

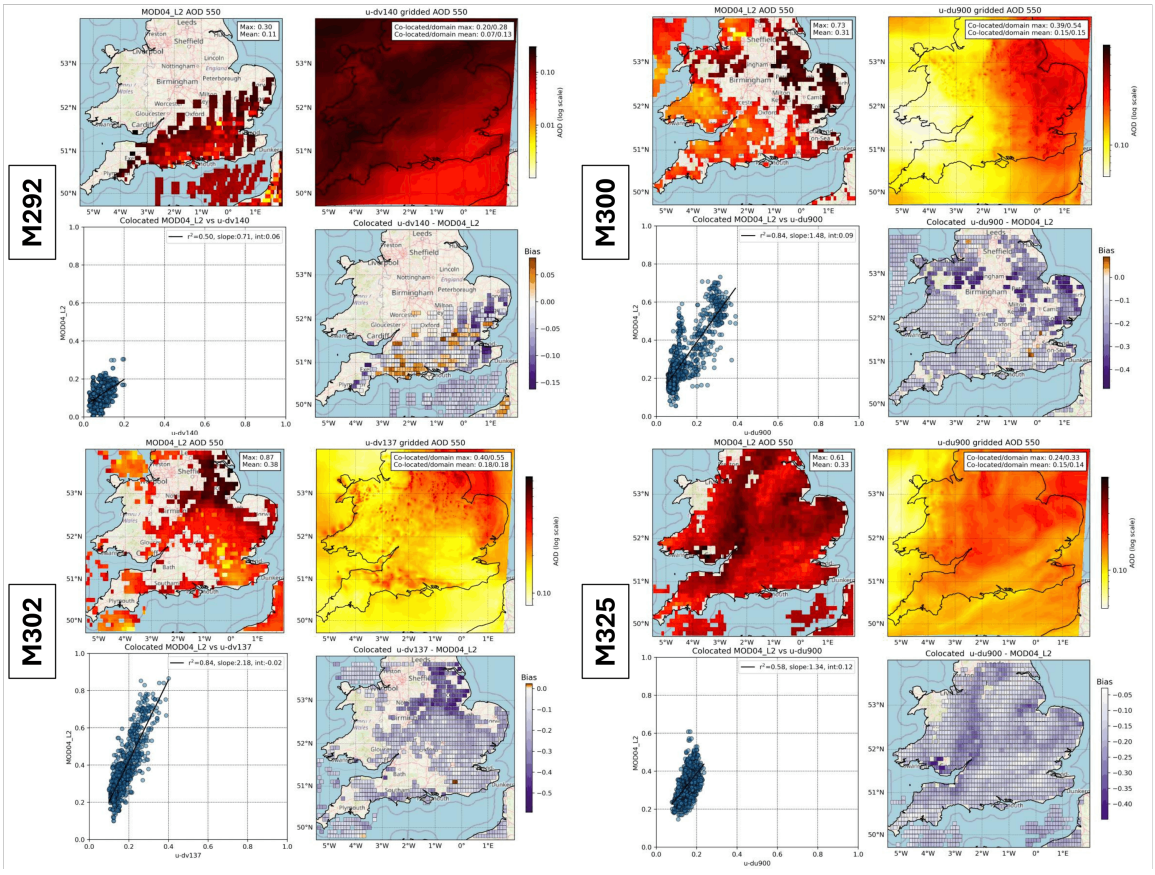

Figure G1. MODIS and SOL/INSOL AOD for case M292 on 14th June 2021, using MODIS overpasses at 10:10, 11:50 and 11:45; case M300 on 20th July 2021, using overpasses at 11:20, 11:25 and 13:00; case M302 on 22nd July 2021, using overpasses at 11:10, 12:40 and 12:45; case M325 on 24th March 2022, using overpasses at 11:20 and 11:25. For each case, panel A shows MODIS 550nm aerosol optical depth, panel B shows SOL/INSOL predicted 550 nm AOD at 13:00 on the case date, C: MODIS against co-located SOL/INSOL AOD and D: mapped difference (co-located SOL/INSOL - MODIS AOD) where blue/orange indicates a model underprediction/overprediction.

Author contributions. ACJ developed the SOL/INSOL model with support from AM, JCK, PF, Adrian Hill and Nicolas Bellouin. AM and AJ designed the model evaluation. AM configured and ran the simulations, wrote the evaluation code and carried out the evaluation. AM prepared the manuscript with contributions from all co-authors. FFM contributed to developing the emission processing code.

Competing interests. The authors declare that they have no conflict of interest.

https://doi.org/10.5194/egusphere-2026-4611
Preprint. Discussion started: 9 November 2026
© Author(s) 2026. CC BY 4.0 License.



Acknowledgements. Anthony Jones and Paul Field were funded by the Met Office Weather and Climate Science for Service Partnership (WCSSP) India project under the International Science Partnerships Fund (ISPF). The authors acknowledge and thank Benjamin Drummond and Pedro Molina-Jimenez for their contributions to the emission processing code and for their assistance in processing the emissions data sets. We acknowledge support from the Clean Air programme (https://www.ukcleanair.org/, last accessed July 2026) in providing the MOASA flight observations. All map tiles have been created with OpenStreetMap under the Open Database License, available at https://www.openstreetmap.org/copyright (Last accessed: 13 July 2026). The authors acknowledge the use of Microsoft Copilot as a writing aid during the preparation of this manuscript, specifically for improving sentence structure, grammar, and readability. The authors were solely responsible for the scientific content, data interpretation, and conclusions of the study, and reviewed all AI-assisted text before submission.

https://doi.org/10.5194/egusphere-2026-4611
Preprint. Discussion started: 9 November 2026
© Author(s) 2026. CC BY 4.0 License.

References

Abdul-Razzak, H. and Ghan, S. J.: A parameterization of aerosol activation: 2. Multiple aerosol types, Journal of Geophysical Research: Atmospheres, 105, 6837–6844, https://doi.org/10.1029/1999JD901161, 2000.

Anurose, T. J., Jayakumar, A., Sandhya, M., Gordon, H., Aryasree, S., Mohandas, S., Bhati, S., and Prasad, V. S.: Unraveling the Mechanism of the Holes in the Blanket of Fog Over the Indo-Gangetic Plains: Are They Driven by Urban Heat Islands or Aerosol?, Geophysical Research Letters, 51, https://doi.org/10.1029/2023GL107252, 2024.

Bagnold, R.: The physics of blown sand and desert dunes. London: Methuen, Progress in Physical Geography Earth and Environment, pp. 91–96, https://doi.org/10.1177/030913339401800105, 1941.

Bellouin, N., Quaas, J., Gryspeerdt, E., Kinne, S., Stier, P., Watson-Parris, D., Boucher, O., Carslaw, K. S., Christensen, M., Daniau, A. L., Dufresne, J. L., Feingold, G., Fiedler, S., Forster, P., Gettelman, A., Haywood, J. M., Lohmann, U., Malavelle, F., Mauritsen, T., McCoy, D. T., Myhre, G., Mülmenstädt, J., Neubauer, D., Possner, A., Rugenstein, M., Sato, Y., Schulz, M., Schwartz, S. E., Sourdeval, O., Storelvmo, T., Toll, V., Winker, D., and Stevens, B.: Bounding Global Aerosol Radiative Forcing of Climate Change, Reviews of Geophysics, 58, 1–45, https://doi.org/10.1029/2019RG000660, 2019.

Bieser, J., Aulinger, A., Matthias, V., Quante, M., and Builtjes, P.: SMOKE for Europe – adaptation, modification and evaluation of a comprehensive emission model for Europe, Geoscientific Model Development, 4, 47–68, https://doi.org/10.5194/gmd-4-47-2011, 2011.

Bohnenstengel, S. I. and Hendry, M. A.: Report on implementation and evaluation of MORUSES in the UKV (PS37), Tech. rep., Met Office, 2016.

Bozzo, A., Remy, S., Benedetti, A., Flemming, J., Bechtold, P., Rodwell, M. J., and Morcrette, J.-J.: Implementation of a CAMS-based aerosol climatology in the IFS, Tech. rep., ECMWF, http://www.ecmwf.int/en/research/publications, 2017.

Bush, M., Flack, D. L. A., Lewis, H. W., Bohnenstengel, S. I., Short, C. J., Franklin, C., Lock, A. P., Best, M., Field, P., McCabe, A., Van Weverberg, K., Berthou, S., Boutle, I., Brooke, J. K., Cole, S., Cooper, S., Dow, G., Edwards, J., Finnenkoetter, A., Furtado, K., Halladay, K., Hanley, K., Hendry, M. A., Hill, A., Jayakumar, A., Jones, R. W., Lean, H., Lee, J. C. K., Malcolm, A., Mittermaier, M., Mohandas, S., Moore, S., Morcrette, C., North, R., Porson, A., Rennie, S., Roberts, N., Roux, B., Sanchez, C., Su, C.-H., Tucker, S., Vosper, S., Walters, D., Warner, J., Webster, S., Weeks, M., Wilkinson, J., Whitall, M., Williams, K. D., and Zhang, H.: The third Met Office Unified Model–JULES Regional Atmosphere and Land Configuration, RAL3, Geoscientific Model Development, 18, 3819–3855, https://doi.org/10.5194/gmd-18-3819-2025, 2025.

Cao, Q., Jiang, B., Shen, X., Lin, W., and Chen, J.: Microphysics effects of anthropogenic aerosols on urban heavy precipitation over the Pearl River Delta, China, Atmospheric Research, 253, 105 478, https://doi.org/10.1016/j.atmosres.2021.105478, 2021.

Chu, D. A., Kaufman, Y. J., Ichoku, C., Remer, L. A., Tanré, D., and Holben, B. N.: Validation of MODIS aerosol optical depth retrieval over land, Geophysical Research Letters, 29, https://doi.org/10.1029/2001GL013205, 2002.

Clark, P. A., Harcourt, S. A., Macpherson, B., Mathison, C. T., Cusack, S., and Naylor, M.: Prediction of visibility and aerosol within the operational Met office unified model.I: Model formulation and variational assimilation, Quarterly Journal of the Royal Meteorological Society, 134, 1801–1816, https://doi.org/10.1002/qj.318, 2008.

DEFRA: Emissions of air pollutants in the UK – Particulate matter (PM10 and PM2.5), https://www.gov.uk/government/statistics/emissions-of-air-pollutants/emissions-of-air-pollutants-in-the-uk-particulate-matter-pm10-and-pm25#trends-in-total-annual-emissions-of-pm10-and-pm25-in-the-uk-1990-to-2024, 2026.

https://doi.org/10.5194/egusphere-2026-4611
Preprint. Discussion started: 9 November 2026
© Author(s) 2026. CC BY 4.0 License.

Denier van der Gon, H., Hendriks, C., Kuenen, J., Segers, A., and Visschedijk, A.: Description of current temporal emission patterns and sensitivity of predicted AQ for temporal emission patterns, Tech. Rep. EU FP7 MACC deliverable report D_D-EMIS_1.3, TNO, Princetonlaan 6, 3584 CB Utrecht, The Netherlands, 2011.

Department for Environment, Food and Rural Affairs: Quality Assurance and Quality Control (QA/QC) Procedures for UK Air Quality Monitoring under the Air Quality Standards Regulations, www.gov.uk/defra, 2023.

Di Antonio, L., Di Biagio, C., Foret, G., Formenti, P., Siour, G., Doussin, J.-F., and Beekmann, M.: Aerosol optical depth climatology from the high-resolution MAIAC product over Europe: differences between major European cities and their surrounding environments, Atmospheric Chemistry and Physics, 23, 12 455–12 475, https://doi.org/10.5194/acp-23-12455-2023, 2023.

ECMWF: CAMS global sea salt aerosol mixing ratios, https://confluence.ecmwf.int/display/CKB/CAMS+global+sea+salt+aerosol+mixing+ratios, 2023.

Esentürk, E., Abraham, N. L., Archer-Nicholls, S., Mitsakou, C., Griffiths, P., Archibald, A., and Pyle, J.: Quasi-Newton methods for atmospheric chemistry simulations: implementation in UKCA UM vn10.8, Geoscientific Model Development, 11, 3089–3108, https://doi.org/10.5194/gmd-11-3089-2018, 2018.

Fecan, F., Marticorena, B., and Bergametti, G.: Parametrization of the increase of the aeolian erosion threshold wind friction velocity due to soil moisture for arid and semi-arid areas, Ann. Geophysicae, 17, 149–157, https://doi.org/10.1007/s00585-999-0149-7, 1999.

Field, P. R., Hill, A., Shipway, B., Furtado, K., Wilkinson, J., Miltenberger, A., Gordon, H., Grosvenor, D. P., Stevens, R., and Van Weverberg, K.: Implementation of a double moment cloud microphysics scheme in the UK met office regional numerical weather prediction model, Quarterly Journal of the Royal Meteorological Society, 149, 703–739, https://doi.org/10.1002/qj.4414, 2023.

Gao, Z. and Zhou, X.: A review of the CAMx, CMAQ, WRF-Chem and NAQPMS models: Application, evaluation and uncertainty factors, Environmental Pollution, 343, 123 183, https://doi.org/https://doi.org/10.1016/j.envpol.2023.123183, 2024.

Gates, W. L., Boyle, J. S., Covey, C., Dease, C. G., Doutriaux, C. M., Drach, R. S., Fiorino, M., Gleckler, P. J., Hnilo, J. J., Marlais, S. M., Phillips, T. J., Potter, G. L., Santer, B. D., Sperber, K. R., Taylor, K. E., and Williams, D. N.: An Overview of the Results of the Atmospheric Model Intercomparison Project (AMIP I), Bulletin of the American Meteorological Society, 80, 29–55, https://doi.org/10.1175/1520-0477(1999)080<0029:AOOTRO>2.0.CO;2, 1999.

Ghosh, P., Boutle, I., Field, P., Hill, A., Jones, A., Mazoyer, M., Evans, K. J., Mahajan, S., Kang, H.-g., Xu, M., Zhang, W., and Asch, N.: High sensitivity of simulated fog properties to parameterized aerosol activation in case studies from ParisFog, Atmospheric Chemistry and Physics, 25, 11 129–11 156, https://doi.org/https://doi.org/10.5194/acp-25-11129-2025, 2025.

Gong, S. L.: A parameterization of sea-salt aerosol source function for sub- and super-micron particles, Global Biogeochemical Cycles, 17, 2003GB002 079, https://doi.org/10.1029/2003GB002079, 2003.

Google LLC: Google Earth, https://earth.google.com/, imagery from the dates: 4/7/2023–6/9/2023, 2023.

Gordon, H., Carslaw, K. S., Hill, A. A., Field, P. R., Abraham, N. L., Beyersdorf, A., Corr-Limoges, C., Ghosh, P., Hemmings, J., Jones, A. C., Sanchez, C., Wang, X., and Wilkinson, J.: NUMAC: Description of the Nested Unified Model With Aerosols and Chemistry, and Evaluation With KORUS-AQ Data, Journal of Advances in Modeling Earth Systems, 15, 1–31, https://doi.org/10.1029/2022MS003457, 2023.

Hu, J., Ying, Q., Chen, J., Mahmud, A., Zhao, Z., Chen, S. H., and Kleeman, M. J.: Particulate air quality model predictions using prognostic vs. diagnostic meteorology in central California, Atmospheric Environment, 44, 215–226, https://doi.org/10.1016/j.atmosenv.2009.10.011, 2010.

https://doi.org/10.5194/egusphere-2026-4611
Preprint. Discussion started: 9 November 2026
© Author(s) 2026. CC BY 4.0 License.

Inness, A., Ades, M., Agustí-Panareda, A., Barré, J., Benedictow, A., Blechschmidt, A.-M., Dominguez, J. J., Engelen, R., Eskes, H., Flemming, J., Huijnen, V., Jones, L., Kipling, Z., Massart, S., Parrington, M., Peuch, V.-H., Razinger, M., Remy, S., Schulz, M., and Suttie, M.: The CAMS reanalysis of atmospheric composition, Atmospheric Chemistry and Physics, 19, 3515–3556, https://doi.org/10.5194/acp-19-3515-2019, 2019.

Jayakumar, A., Anurose, T. J., Bhati, S., Hendry, M. A., Hayman, G., Gordon, H., Field, P., Mohandas, S., Rumbold, H., Yadav, P., Dhangar, N. G., Parde, A., Wagh, S., Ghude, S., Ross, A. N., Smith, D., Dorling, S., George, J. P., Prasad, V. S., and Ravichandran, M.: Development of an Integrated Modeling Framework for Visibility and Air Quality Forecasting in Delhi, Bulletin of the American Meteorological Society, 106, E261–E274, https://doi.org/10.1175/BAMS-D-24-0194.1, 2025.

Jones, A. C., Hill, A., Remy, S., Abraham, N. L., Dalvi, M., Hardacre, C., Hewitt, A. J., Johnson, B., Mulcahy, J. P., and Turnock, S. T.: Exploring the sensitivity of atmospheric nitrate concentrations to nitric acid uptake rate using the Met Office's Unified Model, Atmospheric Chemistry and Physics, 21, 15 901–15 927, https://doi.org/10.5194/acp-21-15901-2021, 2021.

Jones, A. C., Hill, A., Hemmings, J., Lemaitre, P., Quérel, A., Ryder, C. L., and Woodward, S.: Below-cloud scavenging of aerosol by rain: a review of numerical modelling approaches and sensitivity simulations with mineral dust in the Met Office's Unified Model, Atmospheric Chemistry and Physics, 22, 11 381–11 407, https://doi.org/10.5194/acp-22-11381-2022, 2022.

Jones, A. C., Haywood, J. M., Henry, M., and Duffey, A.: Efficacy assessment of Stratospheric Aerosol Scrubbing as a Counter Climate Intervention strategy, https://doi.org/10.5194/egusphere-2025-6332, 2026.

Kettle, A. J., Andreae, M. O., Amouroux, D., Andreae, T. W., Bates, T. S., Berresheim, H., Bingemer, H., Boniforti, R., Curran, M. A. J., DiTullio, G. R., Helas, G., Jones, G. B., Keller, M. D., Kiene, R. P., Leck, C., Levasseur, M., Malin, G., Maspero, M., Matrai, P., McTaggart, A. R., Mihalopoulos, N., Nguyen, B. C., Novo, A., Putaud, J. P., Rapsomanikis, S., Roberts, G., Schebeske, G., Sharma, S., Simó, R., Staubes, R., Turner, S., and Uher, G.: A global database of sea surface dimethylsulfide (DMS) measurements and a procedure to predict sea surface DMS as a function of latitude, longitude, and month, Global Biogeochemical Cycles, 13, 399–444, https://doi.org/10.1029/1999GB900004, 1999.

Liss, P. S. and Merlivat, L.: Air-Sea Gas Exchange Rates: Introduction and Synthesis, in: Buat-Ménard, P. (eds) The Role of Air-Sea Exchange in Geochemical Cycling., no. 185 in NATO ASI Series, Springer, Dordrecht, https://doi.org/https://doi.org/10.1007/978-94-009-4738-2_5, 1986.

Mann, G. W., Carslaw, K. S., Spracklen, D. V., Ridley, D. A., Manktelow, P. T., Chipperfield, M. P., Pickering, S. J., and Johnson, C. E.: Description and evaluation of GLOMAP-mode: A modal global aerosol microphysics model for the UKCA composition-climate model, Geoscientific Model Development, 3, 519–551, https://doi.org/10.5194/gmd-3-519-2010, 2010.

Marticorena, B. and Bergametti, G.: Modeling the atmospheric dust cycle: 1. Design of a soil-derived dust emission scheme, Journal of Geophysical Research: Atmospheres, 100, 16 415–16 430, https://doi.org/10.1029/95JD00690, 1995.

Met Office National Climate Information Centre, Archive, and The National Meteorological Library: Daily Weather Summaries for July 2021, issue: August, 2021.

Metzger, A., Verheggen, B., Dommen, J., Duplissy, J., Prevot, A. S., Weingartner, E., Riipinen, I., Kulmala, M., Spracklen, D. V., Carslaw, K. S., and Baltensperger, U.: Evidence for the role of organics in aerosol particle formation under atmospheric conditions, Proceedings of the National Academy of Sciences of the United States of America, 107, 6646–6651, https://doi.org/10.1073/pnas.0911330107, 2010.

Mikkelsen, A., McCoy, D. T., Eidhammer, T., Gettelman, A., Song, C., Gordon, H., and McCoy, I. L.: Constraining aerosol–cloud adjustments by uniting surface observations with a perturbed parameter ensemble, Atmospheric Chemistry and Physics, 25, 4547–4570, https://doi.org/10.5194/acp-25-4547-2025, 2025.

https://doi.org/10.5194/egusphere-2026-4611
Preprint. Discussion started: 9 November 2026
© Author(s) 2026. CC BY 4.0 License.

Morcrette, J., Boucher, O., Jones, L., Salmond, D., Bechtold, P., Beljaars, A., Benedetti, A., Bonet, A., Kaiser, J. W., Razinger, M., Schulz, M., Serrar, S., Simmons, A. J., Sofiev, M., Suttie, M., Tompkins, A. M., and Untch, A.: Aerosol analysis and forecast in the European Centre for Medium-Range Weather Forecasts Integrated Forecast System: Forward modeling, Journal of Geophysical Research: Atmospheres, 114, 2008JD011 235, https://doi.org/10.1029/2008JD011235, 2009.

Morgenstern, O., Braesicke, P., O'Connor, F. M., Bushell, A. C., Johnson, C. E., Osprey, S. M., and Pyle, J. A.: Evaluation of the new UKCA climate-composition model – Part 1: The stratosphere, Geoscientific Model Development, 2, 43–57, https://doi.org/10.5194/gmd-2-43-2009, 2009.

Mulcahy, J. P., Johnson, C., Jones, C. G., Povey, A. C., Scott, C. E., Sellar, A., Turnock, S. T., Woodhouse, M. T., Abraham, N. L., Andrews, M. B., Bellouin, N., Browse, J., Carslaw, K. S., Dalvi, M., Folberth, G. A., Glover, M., Grosvenor, D. P., Hardacre, C., Hill, R., Johnson, B., Jones, A., Kipling, Z., Mann, G., Mollard, J., O'Connor, F. M., Palmiéri, J., Reddington, C., Rumbold, S. T., Richardson, M., Schutgens, N. A., Stier, P., Stringer, M., Tang, Y., Walton, J., Woodward, S., and Yool, A.: Description and evaluation of aerosol in UKESM1 and HadGEM3-GC3.1 CMIP6 historical simulations, Geoscientific Model Development, 13, 6383–6423, https://doi.org/10.5194/gmd-13-6383-2020, 2020.

Mynard, A., Kent, J., Smith, E. R., Wilson, A., Wivell, K., Nelson, N., Hort, M., Bowles, J., Tiddeman, D., Langridge, J. M., Drummond, B., and Abel, S. J.: Long-term airborne measurements of pollutants over the United Kingdom to support air quality model development and evaluation, Atmospheric Measurement Techniques, 16, 4229–4261, https://doi.org/10.5194/amt-16-4229-2023, 2023.

Neal, L., Agnew, P., Moseley, S., Ordóñez, C., Savage, N., and Tilbee, M.: Application of a statistical post-processing technique to a gridded, operational, air quality forecast, Atmospheric Environment, 98, 385–393, https://doi.org/10.1016/j.atmosenv.2014.09.004, 2014.

Neal, L. S., Dalvi, M., Folberth, G., McInnes, R. N., Agnew, P., O'Connor, F. M., Savage, N. H., and Tilbee, M.: A description and evaluation of an air quality model nested within global and regional composition-climate models using MetUM, Geoscientific Model Development, 10, 3941–3962, https://doi.org/10.5194/gmd-10-3941-2017, iSBN: 1039412017, 2017.

Reddy, M. S., Boucher, O., Bellouin, N., Schulz, M., Balkanski, Y., Dufresne, J., and Pham, M.: Estimates of global multicomponent aerosol optical depth and direct radiative perturbation in the Laboratoire de Météorologie Dynamique general circulation model, Journal of Geophysical Research: Atmospheres, 110, 2004JD004 757, https://doi.org/10.1029/2004JD004757, 2005.

Savage, N. H., Agnew, P., Davis, L. S., Ordóñez, C., Thorpe, R., Johnson, C. E., O'Connor, F. M., and Dalvi, M.: Air quality modelling using the Met Office Unified Model (AQUM OS24-26): Model description and initial evaluation, Geoscientific Model Development, 6, 353–372, https://doi.org/10.5194/gmd-6-353-2013, 2013.

Seinfeld, J. H. and Pandis, S. N.: Atmospheric Chemistry and Physics,, Wiley, New York, USA,, ISBN ISBN-10 0471178152, ISBN13 978-0471178156, 1998.

Sindelarova, K., Granier, C., Bouarar, I., Guenther, A., Tilmes, S., Stavrakou, T., Müller, J.-F., Kuhn, U., Stefani, P., and Knorr, W.: Global data set of biogenic VOC emissions calculated by the MEGAN model over the last 30 years, Atmospheric Chemistry and Physics, 14, 9317–9341, https://doi.org/10.5194/acp-14-9317-2014, 2014.

Stevens, B., Fiedler, S., Kinne, S., Peters, K., Rast, S., Müsse, J., Smith, S. J., and Mauritsen, T.: MACv2-SP: A parameterization of anthropogenic aerosol optical properties and an associated Twomey effect for use in CMIP6, Geoscientific Model Development, 10, 433–452, https://doi.org/10.5194/gmd-10-433-2017, 2017.

Tang, Y., Lean, H. W., and Bornemann, J.: The benefits of the Met Office variable resolution NWP model for forecasting convection, Meteorological Applications, 20, 417–426, https://doi.org/10.1002/met.1300, 2013.

topographic-map.com: topographic-map.com, https://en-gb.topographic-map.com/, 2026.

https://doi.org/10.5194/egusphere-2026-4611
Preprint. Discussion started: 9 November 2026
© Author(s) 2026. CC BY 4.0 License.

UKRI: Integrated Research Observation System for Clean Air (OSCA), https://gtr.ukri.org/projects?ref=NE%2FT001984%2F1, publication Title: [internet], 2021.

Vehkamäki, H., Kulmala, M., Napari, I., Lehtinen, K. E. J., Timmreck, C., Noppel, M., and Laaksonen, A.: An improved parameterization for sulfuric acid–water nucleation rates for tropospheric and stratospheric conditions, Journal of Geophysical Research: Atmospheres, 107, https://doi.org/10.1029/2002JD002184, 2002.

Voigt, A., Stevens, B., Bony, S., and Boucher, O.: Easy Aerosol: a modeling framework to study robustness and sources of uncertainties in aerosol-induced changes of the large-scale atmospheric circulation, https://www.wcrp-climate.org/images/grand_challenges/clouds/documents/easyaerosol_projectdescription_expprotocol.pdf, 2014.

Walters, D., Baran, A. J., Boutle, I., Brooks, M., Earnshaw, P., Edwards, J., Furtado, K., Hill, P., Lock, A., Manners, J., Morcrette, C., Mulcahy, J., Sanchez, C., Smith, C., Stratton, R., Tennant, W., Tomassini, L., Van Weverberg, K., Vosper, S., Willett, M., Browse, J., Bushell, A., Carslaw, K., Dalvi, M., Essery, R., Gedney, N., Hardiman, S., Johnson, B., Johnson, C., Jones, A., Jones, C., Mann, G., Milton, S., Rumbold, H., Sellar, A., Ujiie, M., Whitall, M., Williams, K., and Zerroukat, M.: The Met Office Unified Model Global Atmosphere 7.0/7.1 and JULES Global Land 7.0 configurations, Geoscientific Model Development, 12, 1909–1963, https://doi.org/10.5194/gmd-12-1909-2019, 2019.

Wang, X., Carslaw, K. S., Grosvenor, D. P., and Gordon, H.: Weak influence of anthropogenic emissions on aerosol , cloud , and rain in the wet season of the Amazon rainforest, Atmospheric Chemistry and Physics, pp. 9685–9717, 2025.

Warren, E., Charlton-Perez, C., Kotthaus, S., Marenco, F., Ryder, C., Johnson, B., Green, D., Lean, H., Ballard, S., and Grimmond, S.: Observed aerosol characteristics to improve forward-modelled attenuated backscatter in urban areas, Atmospheric Environment, 224, 117 177, https://doi.org/10.1016/j.atmosenv.2019.117177, 2020.

Watson, N., Allan, J. D., and Flynn, M.: Integrated Research Observation System for Clean Air (OCSA): Birmingham, Manchester and London air quality supersites data collection, https://catalogue.ceda.ac.uk/uuid/65b50d3348cb4745bb7acfcf6f2057b8/, 2023.

Wei, J., Li, Z., Sun, L., Peng, Y., Liu, L., He, L., Qin, W., and Cribb, M.: MODIS Collection 6.1 3 km resolution aerosol optical depth product: global evaluation and uncertainty analysis, Atmospheric Environment, 240, 117 768, https://doi.org/10.1016/j.atmosenv.2020.117768, 2020.

Weiss, P., Herbert, R., and Stier, P.: ICON-HAM-lite: simulating the Earth system with interactive aerosols at kilometer scales, Geoscientific Model Development, https://doi.org/10.5194/egusphere-2024-3325, 2024.

Willett, M. R., Brooks, M., Bushell, A., Earnshaw, P., Smith, S., Tomassini, L., Best, M., Boutle, I., Brooke, J., Edwards, J. M., Furtado, K., Hardacre, C., Hartley, A. J., Hewitt, A., Johnson, B., Lock, A., Malcolm, A., Mulcahy, J., Müller, E., Rumbold, H., Rooney, G. G., Sellar, A., Ujiie, M., Van Niekerk, A., Wiltshire, A., and Whitall, M.: The Met Office Unified Model Global Atmosphere 8.0 and JULES Global Land 9.0 configurations, https://doi.org/10.5194/egusphere-2025-1829, 2025.

Woodward, S.: Mineral Dust in HadGEM2, Hadley Centre Technical Note 87, Met Office Hadley Centre, 2011.

Woodward, S., Sellar, A. A., Tang, Y., Stringer, M., Yool, A., Robertson, E., and Wiltshire, A.: The simulation of mineral dust in the United Kingdom Earth System Model UKESM1, Atmospheric Chemistry and Physics, 22, 14 503–14 528, https://doi.org/10.5194/acp-22-14503-2022, 2022.

Yang, J., Ke, H., Gong, S., Wang, Y., Zhang, L., Zhou, C., Mo, J., and You, Y.: Enhanced Forecasting and Assessment of Urban Air Quality by an Automated Machine Learning System: The AI-Air, Earth and Space Science, 12, https://doi.org/10.1029/2024EA003942, 2025.

Zhu, Q., Schwantes, R. H., Coggon, M., Harkins, C., Schnell, J., He, J., Pye, H. O. T., Li, M., Baker, B., Moon, Z., Ahmadov, R., Pfannerstill, E. Y., Place, B., Wooldridge, P., Schulze, B. C., Arata, C., Bucholtz, A., Seinfeld, J. H., Warneke, C., Stockwell, C. E., Xu, L., Zuraski,

https://doi.org/10.5194/egusphere-2026-4611
Preprint. Discussion started: 9 November 2026
© Author(s) 2026. CC BY 4.0 License.



K., Robinson, M. A., Neuman, J. A., Veres, P. R., Peischl, J., Brown, S. S., Goldstein, A. H., Cohen, R. C., and McDonald, B. C.: A better representation of volatile organic compound chemistry in WRF-Chem and its impact on ozone over Los Angeles, Atmospheric Chemistry and Physics, 24, 5265–5286, https://doi.org/10.5194/acp-24-5265-2024, 2024.